The design of a simulation model of the RF front-end of an OFDM-based WLAN transceiver

van Eerd, R.J.

Award date:
2001

TU/e technische universiteit eindhoven

Department of Electrical Engineering
Division of Telecommunication Technology and Electromagnetism

The Design of a Simulation Model of the RF Front-end of an OFDM-based WLAN Transceiver

by R.J. van Eerd

Master's thesis report
Master's thesis performed from January 2nd to September 28th 2001
Master's thesis performed at Philips Semiconductors Systems Lab Eindhoven
Master's thesis supervised by prof. dr. ir. G. Brussaard, TU/e
ir. W. van Houtum, PS-SLE
ing. R. van Apeldoorn, PS-SLE

Summary

In recent years there has been an increase in the use of mobile devices. A Wireless Local Area Network (WLAN) can provide data exchange and network access for these devices without the loss of mobility. In 1997, the Institute of Electrical and Electronics Engineers (IEEE) adopted the IEEE 802.11 standard, the first standard for WLANs. In 1999, the IEEE adopted two extensions to the original standard to provide higher data rates. One of these extensions, IEEE 802.11a, uses a complete new physical layer implementation based on Orthogonal Frequency Division Multiplexing (OFDM).
Currently, at the Philips Semiconductors Systems Lab Eindhoven, a IEEE 802.11a compliant modem is being designed. A partial simulation model of the current design existed however a simulation model of the RF front-end was not available. The design of a simulation model of the RF front-end is the subject of the Master's thesis performed by the author as part of the author's study at the Department of Electrical Engineering at the Eindhoven University of Technology. During the Master's thesis, the principles of OFDM modulation and the current modem design have been studied and the effects of the components of the RF front-end on the OFDM signal, especially the effects of imperfections, have been determined. Based on these results, a simulation model of the RF front-end has been created and some simulations have been performed. The simulations indicate that the current design complies to the requirements set by the IEEE 802.11a standard in most cases. However, for high transmit and received powers, the Power Amplifier (PA) of the transmitter and the Low Noise Amplifier (LNA) of the receiver are operated close to the compression point, which introduces much intermodulation interference. These problems can be solved by using another PA or by using a larger back-off for the LNA.
The simulation model was based on limited specifications. If additional specifications become available the simulation model can be improved. Additional simulations should be performed to determine the effect of all imperfections on the performance and to determine what imperfections can be tolerated for the required performance of the current modem design.

Preface

This report describes the work I performed during my Master's thesis at the Philips Semiconductors Systems Lab Eindhoven (PS-SLE). And although you will find only my name on the title page as the author, I could not have done this work without the aid of various people, who I would like to thank for their support. First of all, I would like to thank my graduate professor G. Brussaard of the Eindhoven University of Technology, who made it possible to perform my Master's thesis externally to the University. I especially appreciated his frequent visits to the PS-SLE, which showed his interest in the work I was doing. I would also like to thank my supervisors of the PS-SLE, W. van Houtum and R. van Apeldoorn, who were always ready to assist me when I encountered problems. Other people also contributed in various ways, like Brian de Bart, Marc Arends, Stefan Crijns and Oswald Moonen, all of the PS-SLE. Finally I would like to thank my co-workers who made my stay at the PS-SLE a pleasant time.

Rutger van Eerd
Eindhoven, September 28th 2001

Contents

1 Introduction

In recent years, there has been an increase in the use of mobile devices, including notebook computers. Notebooks are more convenient to use then desktop computers as they can be easily moved from one location to another and they do not require access to a power outlet. Just like desktops, notebooks need to exchange data with other computers and need access to network resources, such as printers and storage devices. A Wireless Local Area Network (WLAN) can provide data exchange and network access without the loss of mobility [10].
In 1997, the Institute of Electrical and Electronics Engineers (IEEE) adopted the IEEE 802.11 standard, the first standard for WLANs. The standard is designed to be indistinguishable from fixed LANs for the higher networks layers. The standard provides reliable data communications at data rates up to 2 Mbps. The standard supports mobility and power saving operations to make optimal use of the advantages of mobile devices [11].
In 1999, the IEEE adopted two extensions to the IEEE 802.11 standard. The first, IEEE 802.11a, uses a complete new physical layer implementation based on Orthogonal Frequency Division Multiplexing (OFDM) and provides data rates up to 54 Mbps. The second, IEEE 802.11b, is an extension to one of the physical layer implementations of the original standard and provides data rates up to 11 Mbps [11].
Currently, at the Philips Semiconductors Systems Lab Eindhoven (PS-SLE), a IEEE 802.11a compliant modem is being designed. The modem implements the OFDM physical layer and consists of two distinct parts: a digital baseband module and an analogue Radio Frequency (RF) front-end. At the transmitter, the baseband module uses the supplied binary data to generate the OFDM signal at baseband and the RF front-end converts the baseband signal to the correct RF frequency. At the receiver, the reverse process takes place. The RF front-end converts the received OFDM signal from the RF to baseband and the baseband module recovers the transmitted binary data. The baseband module is designed internally at the PS-SLE and a simulation model exists. The RF front-end is designed externally; no simulation model exists and only limited specifications are available. However, a simulation model of the RF front-end is required to determine the performance of the entire modem.
The design of a simulation model of the RF front-end is the subject of this Master's thesis report. The Master's thesis was performed by the author as part of the author's study at the Department of Electrical Engineering at the Eindhoven University of Technology. The goals of the Master's thesis are as follows

- Become familiar with the principles of OFDM modulation.
- Become familiar with the current design of the modem, especially the RF front-end.

- Determine how the components of the RF front-end effect the OFDM signal, especially the effect of imperfections on the OFDM signal.
- Create simulation models of the components of the RF front-end, including the imperfections. The detail of the simulation model will be determined by the limited specifications that are available.
- Create a simulation model of the entire RF front-end.
- Perform simulations to determine the performance of the RF front-end.
- Perform simulations to determine the performance of the entire modem.

The simulation model designed during the Master's thesis and presented in this report is created using the Cadence® Signal Processing Worksystem (SPW) design environment.
The report is organised as follows. Chapter 2 presents a short introduction of digital modulation, single carrier modulation and limitations to practical achievable data rates with single carrier digital communication systems. Chapter 3 discusses the principles of OFDM modulation and the reasons why OFDM modulation is more suited for high-speed digital communication systems than single carrier modulation. It also discusses why synchronisation is required because of transmitter and receiver imperfections and how synchronisation can be performed. Chapter 4 gives an overview of the IEEE 802.11 standards and presents relevant information about the IEEE 802.11a standard. Chapter 5 discusses the current design of the baseband module and derives a simulation model of the baseband module. Chapter 6 discusses the current design of the RF front-end and derives a simulation model of the RF front-end. Chapter 7 describes the simulations that were performed and presents and interprets the results. Chapter 8 ends the report with conclusions and recommendations.

2
Single Carrier Modulation

Digital communication systems use many different ways to modulate digital data onto a carrier. However, all modulation schemes are based on one or a combination of the basic modulation types Amplitude Shift Keying (ASK), Frequency Shift Keying (FSK) and Phase Shift Keying (PSK). Many current systems use the Quadrature Amplitude Modulation (QAM) scheme, which is a combination of ASK and PSK. Using the QAM modulation scheme, the modulation symbols have M distinct states and each symbol represents $k = \log_2 M$ bits of information. Each symbol state is determined by the amplitude and phase and the states are often represented as a complex value $I + jQ$, where the real part I is the *in-phase component* and the imaginary part Q is the *quadrature component*. The symbol states can be graphically represented in a *constellation diagram*, as shown in Figure 1 [1], [2].

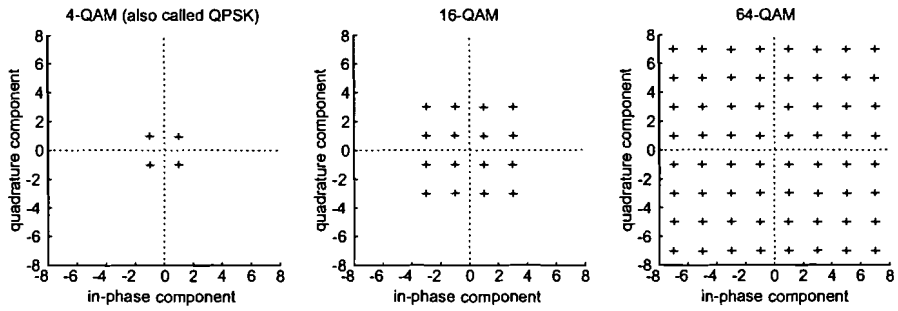

Figure 1: QAM constellations.

Many digital communication systems use a single carrier to transmit the modulation symbols. Figure 2 shows the block diagram of a single carrier modulator.

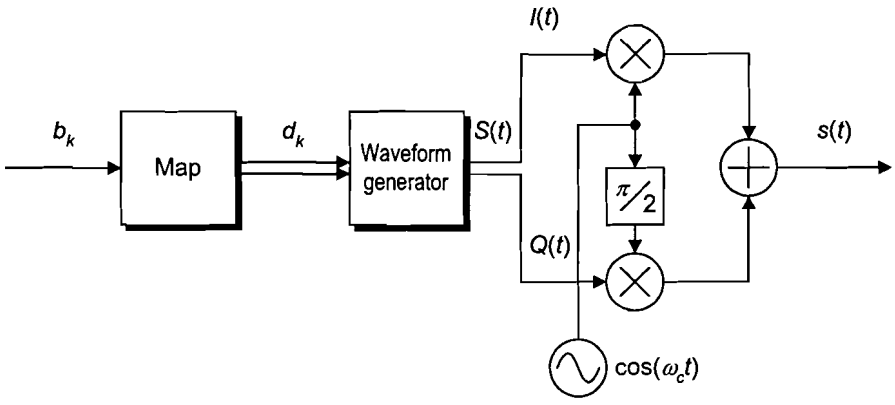

Figure 2: Single carrier modulator.

The binary data symbols b_k are mapped to the modulation symbols d_k, e.g. QAM symbols. Based on the modulation symbols, symbol waveforms are generated. The symbol waveforms are then modulated onto a carrier using a *quadrature*

modulator, which multiplies the in-phase component with the oscillator signal at the carrier frequency ω_c and the quadrature component with the $\pi/2$ phase-shifted oscillator signal. The output of quadrature modulator is given by

$$\begin{aligned} s(t) &= I(t)\cos(\omega_c t) - Q(t)\sin(\omega_c t) \\ &= \mathrm{Re}\left\{\left[I(t) + jQ(t)\right]e^{j\omega_c t}\right\} \\ &= \mathrm{Re}\left\{S(t)e^{j\omega_c t}\right\} \end{aligned} \tag{1}$$

In this equation, the complex baseband signal $S(t)$ is the *complex envelope* of the passband, quadrature modulated signal $s(t)$. The complex envelope is often used in literature to represent signals.
Single carrier systems can operate at various data rates, however there are limits to practical achievable data rates, as described in the following paragraphs.

2.1 Limited Bandwidth

The data rate of a single carrier digital communication system can be increased by reducing the symbol duration T_s and thus increasing the symbol rate $1/T_s$. This will also increase the occupied bandwidth as this is proportional to the symbol rate. However, the bandwidth a signal may occupy is usually limited—because of design considerations or regulations—and thus the symbol rate can not be increased without bounds [1].

2.2 Noise

The data rate of a single carrier digital communication system can also be increased by increasing the number of symbol states. This will reduce the distance between the different symbol states if the average signal power is not changed. As noise is added to the signal during transmission, this will increase the chance of detecting a symbol state incorrectly. To achieve the same Symbol Error Rate (SER) or Bit Error Rate (BER) the Signal-to-Noise Ratio (SNR) of the signal needs to be increased. However, the transmission power is often limited—because of design considerations or regulations—and thus the number of symbol states can not be increased without bounds [1].

2.3 Multipath

Reflections and scattering cause the signal to arrive at the receiver along different paths. This kind of propagation is called *multipath* propagation and is illustrated in Figure 3. As the paths will have different lengths, the corresponding signals will have different propagation delays. A multipath channel is often characterised by the *rms delay spread* σ_τ, which is the standard deviation of the propagation delays of the various received signals [2].
The coherence bandwidth characterises a multipath channel in the frequency domain and is proportional to the reciprocal of the rms delay spread. The *coherence bandwidth* B_c is a statistical measure of the range of frequencies over which the channel can be considered "flat", i.e. has approximately equal gain and linear phase. If the coherence bandwidth is much larger than the signal bandwidth, the shape of the signal spectrum is not changed and the signal undergoes *flat fading*. A flat fading channel has a channel gain that changes over time and can cause deep fades. For a flat fading channel, the rms delay spread is

much smaller than the symbol duration. If the coherence bandwidth is smaller than the signal bandwidth, the shape of the signal spectrum is not preserved and the signal undergoes *frequency selective fading*. A frequency selective fading channel induces Inter-Symbol Interference (ISI) because the rms delay spread is larger than the symbol duration [2].
Multipath propagation sets a limit for the symbol rate as the SER will increase because of ISI if the rms delay spread becomes large compared to the symbol duration.

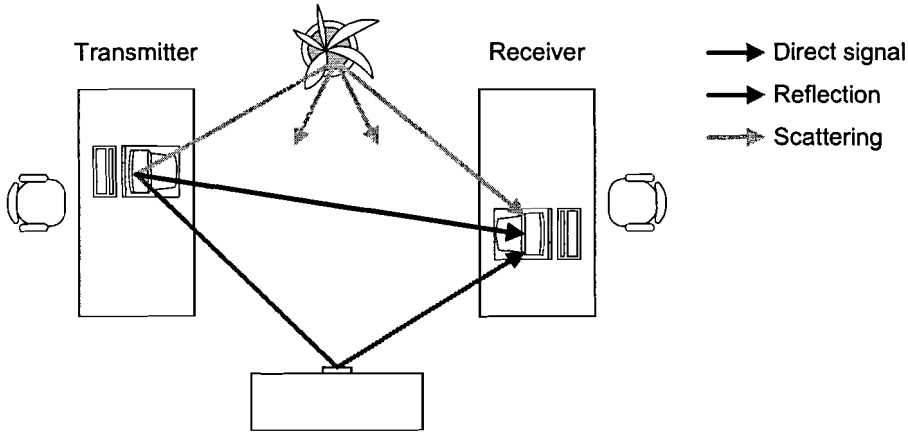

Figure 3: Multipath.

2.4 Interference

Interference can cause the entire link to fail, which requires retransmission of the lost symbols. This reduces the actual data rate that can be achieved by the communication system. Error correction coding can be used to reduce the need for retransmissions but this adds redundancy which also reduces the actual data rate.

3
Orthogonal Frequency Division Multiplexing

The limitations to practical achievable data rates make single carrier systems less suitable for high-speed wireless data communication [1]. A modulation technique that overcomes some of the problems discussed in the previous chapter is OFDM. OFDM is a modulation technique that splits a high-speed data stream into a number of lower-speed data streams that are modulated on different subcarriers. The subcarriers are orthogonal to each other which makes efficient use of bandwidth possible. The lower-speed data streams have a longer symbol duration which makes OFDM more robust to delay spread. The use of multiple subcarriers in combination with error correction coding makes OFDM more resistant to frequency selective fading and narrow-band interference. This chapter describes the OFDM modulation technique and its advantages and disadvantages.

3.1 Basics of OFDM Modulation

As stated before, OFDM uses a number of subcarriers to transmit the data stream. In a classical multicarrier system the subcarriers are chosen in such a way that spectral overlap is avoided and Inter-Channel Interference (ICI) is eliminated. This leads to inefficient use of bandwidth as the subcarriers are spaced at large distances. OFDM uses a different approach.

When a rectangular pulse is modulated onto a carrier, the spectrum of the pulse is centred at the carrier frequency. The spectrum of a rectangular pulse with unit amplitude and a duration of T_s is given by

$$\Pi(f) = T_s \frac{\sin(\pi f T_s)}{\pi f T_s} = T_s \,\mathrm{sinc}(f T_s) \tag{2}$$

The spectrum $\Pi(f)$ is zero for all frequencies $f = n/T_s$ with $n \neq 0$. Thus when rectangular pulses are modulated on multiple subcarriers that are spaced $f_s = 1/T_s$ in frequency, the subcarriers experience no mutual interference. Hence the subcarriers are *orthogonal* with respect to each other and no ICI occurs. This is illustrated in Figure 4 [3].

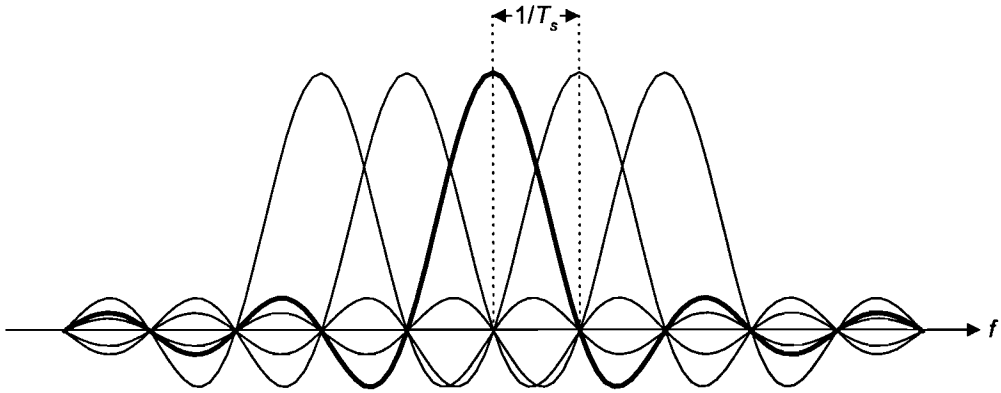

Figure 4: Spectra of orthogonal subcarriers.

The block diagram of an OFDM modulator is shown in Figure 5. The binary data symbols b_k are mapped to the modulation symbols d_k. The modulation symbols are modulated onto N_s subcarriers that are spaced f_s in frequency. The modulated subcarriers are then summed to generate the complex baseband signal $S(t)$, which is the complex envelope of the passband OFDM signal $s(t)$. The complex baseband signal is applied to the quadrature modulator to generate the passband OFDM signal [3].

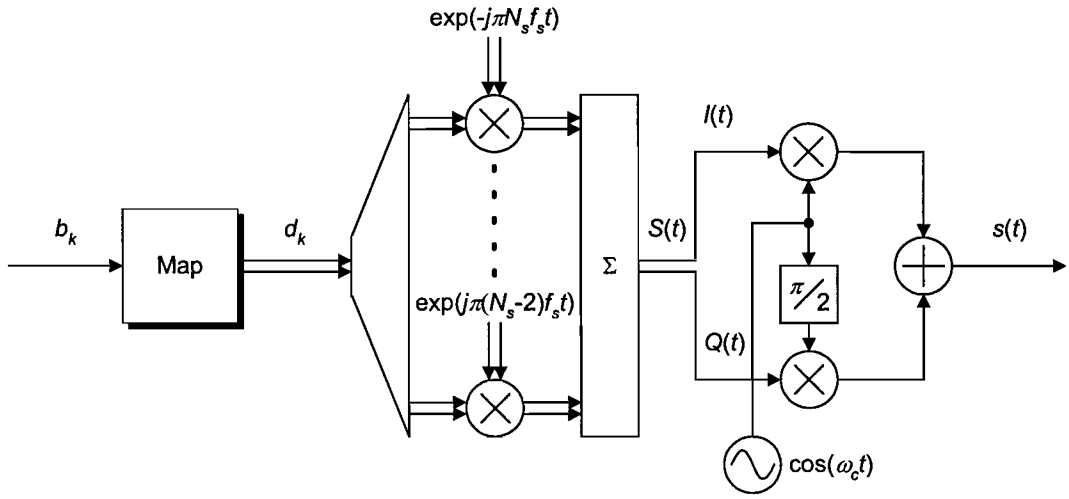

Figure 5: OFDM modulator.

The elimination of ICI in OFDM can be proven by looking at a single OFDM symbol. The complex envelope of a single OFDM symbol starting at $t = 0$ is given by

$$S(t) = \sum_{i=-\frac{N_s}{2}}^{\frac{N_s}{2}-1} d_{i+\frac{N_s}{2}} \exp(j2\pi \frac{i}{T_s} t), 0 \le t \le T_s \tag{3}$$

The OFDM symbol has a duration of T_s seconds. Each subcarrier has an integer number of cycles in the interval T_s and the number of cycles between adjacent subcarriers differs exactly by one. It will be shown that this property accounts for the orthogonality of the subcarriers.

At the receiver, the kth subcarrier is demodulated by downconverting the signal with a frequency of k/T_s and then integrating the signal over T_s seconds as given by

$$R_k(t) = \int_0^{T_s} \exp(-j2\pi \frac{k}{T_s} t) \sum_{i=-\frac{N_s}{2}}^{\frac{N_s}{2}-1} d_{i+\frac{N_s}{2}} \exp(j2\pi \frac{i}{T_s} t) dt$$
$$= \sum_{i=-\frac{N_s}{2}}^{\frac{N_s}{2}-1} d_{i+\frac{N_s}{2}} \int_0^{T_s} \exp(j2\pi \frac{i-k}{T_s} t) dt = d_{k+\frac{N_s}{2}} T_s \quad (4)$$

For the kth subcarrier, the integration gives the corresponding modulation symbol. For all other subcarriers the integration is zero because the frequency difference $(i - k)/T_s$ produces an integer number of cycles within the integration interval T_s. Therefor the modulation symbol transmitted on subcarrier k can be successfully recovered [3].
The OFDM signal in equation (3) is actually the inverse Fourier transform of N_s modulation symbols. This means that OFDM modulation can be efficiently implemented by the Inverse Fast Fourier Transform (IFFT) in discrete time. For example, to create an OFDM symbol with eight subcarriers an eight point IFFT can be used. Accordingly, OFDM demodulation can be implemented by the FFT [3].

3.1.1 Guard Time

As OFDM uses a number of lower rate subcarriers to transmit the data stream, the symbol duration is increased. This reduces the impact of ISI. ISI can be reduced by adding a *guard time* to each OFDM symbol. As long as the guard time is larger than the delay spread no ISI will occur, as the FFT interval can be shifted such that only the current symbol falls within the FFT interval. The guard time could consist of no signal at all but this can result in ICI as is illustrated in Figure 6. Subcarrier $k + 1$ has no integer number of cycles within the integration interval and when the kth subcarrier is demodulated this will introduce interference.

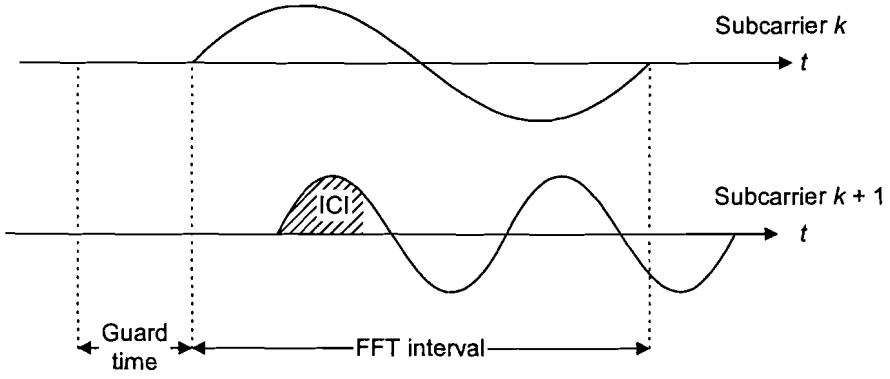

Figure 6: ICI caused by zero signal guard time.

To eliminate ICI, the OFDM symbol is cyclically extended in the guard time to ensure that all subcarriers have an integer number of cycles within the integration interval [3].

3.1.2 Windowing

When multiple OFDM symbols are transmitted after each other there can be sharp phase transitions at the symbol boundaries because the subcarriers are modulated by modulation symbols. This causes the out-of-band spectrum to decrease very slowly. To reduce this effect, windowing is often used to make the amplitude go smoothly to zero at the symbol boundaries. This, however, reduces the delay spread tolerance as the subcarriers are no longer orthogonal in the region where the amplitudes are attenuated [3].

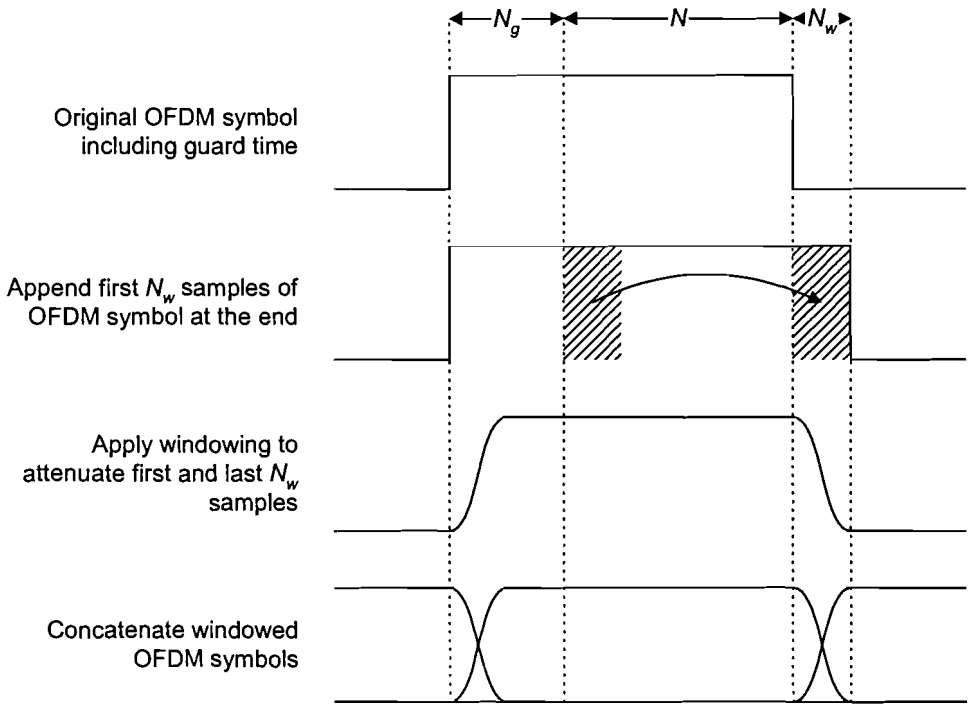

Figure 7: Windowing.

Windowing is usually performed as illustrated in Figure 7. Suppose a N-point IFFT is used to generate the OFDM symbol, in which case the symbol duration is N samples. A guard time is added by inserting the last N_g samples at the start, which leads to a total symbol length of $N + N_g$ samples. Suppose a window with a roll-off region of N_w samples is used. Then, the first N_w samples of the OFDM symbol are appended to the end and windowing is applied. Because the roll-off region is N_w samples long, only the first and last N_w samples are attenuated. Finally, consecutive OFDM symbols are concatenated, such that there is an overlap region of N_w samples [3].

3.1.3 Coding and Interleaving

In a single-carrier modulation scheme, frequency selective fading and narrow-band interference can cause the entire link to fail but in a multicarrier modulation scheme only some of the subcarriers will be affected. Forward Error

Correction (FEC) coding across the subcarriers is often used to correct the errors caused by the few affected subcarriers. Frequency selective fading and narrow-band interference will usually affect adjacent subcarriers. If sequential bits are transmitted on adjacent subcarriers, errors will occur in bursts rather than being randomly scattered. As some FEC methods can not handle such a burst-error, interleaving is often used. By using interleaving, the coded bits are reordered so that adjacent bits will be transmitted on non-adjacent subcarriers [3].

3.2 Synchronisation

An OFDM demodulator can retrieve the transmitted modulation symbols d_k only if it uses the same symbol timing, carrier frequency and carrier phase as the transmitter. These can not be known beforehand at the receiver, as they are influenced by transmitter and receiver imperfections and the properties of the channel. Hence the receiver needs to perform synchronisation to estimate and correct for the carrier properties and symbol timing. The following paragraphs explain why synchronisation is needed and how it can be implemented.

3.2.1 Phase Noise

The transmitter and receiver use oscillators to generate the carrier signal. Practical oscillators suffer from *phase noise*, which means that the signal they produce does not have a perfectly constant frequency. An oscillator signal including phase noise can be represented as

$$y(t) = \cos(\omega_c t + \varphi_n(t)) \tag{5}$$

In this equation, ω_c is the oscillator frequency and $\varphi_n(t)$ is the phase noise signal. Phase noise adds a phase offset to the subcarriers. This results in a phase rotation of the modulation symbols. As the phase offset is the same for all subcarriers of a single OFDM symbol, it can be estimated and corrected if some of the subcarriers are *pilot subcarriers*, which contain reference information. As the phase offset is common to all subcarriers of a single OFDM symbol, this effect is often referred to as the Common Phase Error (CPE) [3], [4].
Phase noise also causes ICI because the subcarriers are no longer spaced at exactly f_s in frequency. As this effect can not be compensated for it sets a minimum requirement for the quality of the oscillator [3], [4].
The Power Spectral Density (PSD) of the phase noise signal $\varphi_n(t)$ is often modelled as [3], [5], [6]

$$\Phi_n(f) = \frac{K}{\pi\beta} \frac{1}{1+(f/\beta)^2} \tag{6}$$

The equation specifies the PSD relative to the carrier frequency. In this equation, β is the 3-dB linewidth of the phase noise spectrum and K is the total integrated phase noise power, which is often specified relative to the carrier power in dBc. According to [4], the CPE is mainly caused by the low-frequency components—up to about the subcarrier spacing f_s—and ICI is mainly caused by the high-frequency components of the phase noise spectrum. Hence, if the phase noise spectrum is narrow-band with respect to the subcarrier spacing there will be a small amount of ICI and mainly CPE. If the phase noise spectrum is broad with respect to the subcarrier spacing there will be a small CPE and mainly ICI. As

the CPE can be compensated and ICI can not, an oscillator with a narrow-band phase noise spectrum is preferred for OFDM modulation.

3.2.2 Frequency Offset

When the transmitter and receiver do not use the same carrier frequency, a frequency offset exists. Frequency offset causes ICI because of loss of orthogonality. The amount of ICI is proportional to the frequency offset and inversely proportional to the subcarrier spacing. The middle subcarriers experience approximately twice as much interference as the egde subcarriers, because the middle subcarriers have interfering subcarriers on both sides. The frequency offset needs to be estimated and corrected to reduce the SNR degradation caused by ICI [3], [7].
An offset in the receiver sampling clock frequency has similar effects as a carrier frequency offset [3], [7].

3.2.3 Timing Offset

As discussed earlier in this chapter, the guard time makes OFDM very robust with respect to timing errors. As long as the FFT interval completely falls within the flat part of the symbol window no ICI or ISI will occur. Figure 8 shows that in the case of a large delay spread, ISI is caused by the previous symbol and ICI is caused by the delayed current symbol. According to [3] an optimal timing instant can be determined that decreases ISI and ICI and increases the robustness with respect to delay spread.

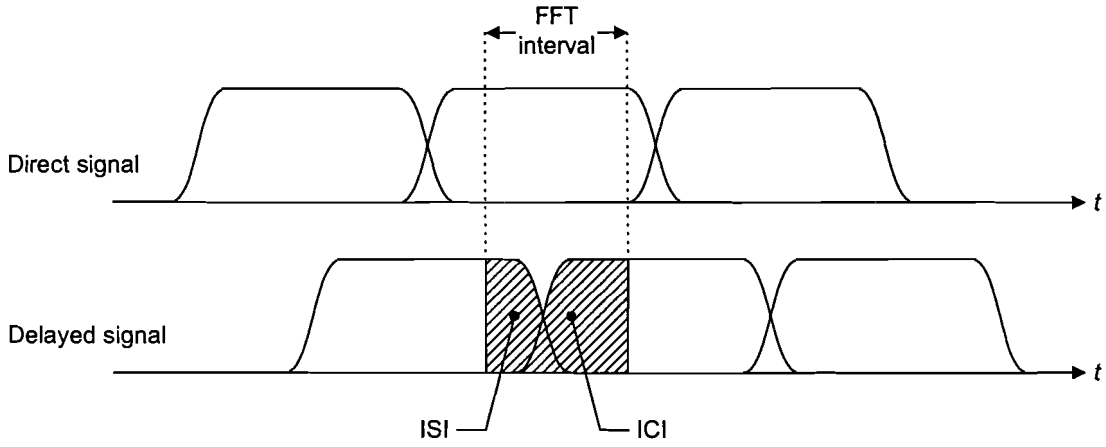

Figure 8: ISI and ICI caused by multipath.

A timing offset leads to a phase shift that is different for each subcarrier. The phase shift of subcarrier k for a timing offset of τ seconds or n samples is given by

$$\Delta\varphi_k = 2\pi f_k \tau = 2\pi \frac{k}{N} n \tag{7}$$

In this equation, N is the FFT size. This phase shift adds to any phase shift caused by multipath propagation. A coherent receiver needs to estimate and correct for the phase shift of each individual subcarrier in order to correctly retrieve the transmitted complex symbols [3], [8].

3.2.4 Synchronisation Methods

Because of frequency, phase and timing offsets synchronisation is needed to correctly demodulate a received OFDM signal.

According to [8], frequency and timing offsets can be estimated and corrected after the FFT has been performed. Since the initial offsets can be arbitrarily large, the initial FFT output will contain a significant amount of interference. Several iterations would be needed for correct synchronisation which leads to a long acquisition time. For systems that use bursty transmissions—such as WLANs—a long acquisition time is unacceptable. Hence synchronisation should be performed before the FFT.

Synchronisation can be performed before the FFT by using the guard time. Since the guard time contains a cyclic extension of the OFDM symbol the first T_g seconds of the OFDM symbol are identical to the last part. When a T_g long part of the received signal is correlated with a part that is T_s seconds delayed, the resulting signal will contain a peak for each OFDM symbol. This method, however, only works well when a large number of subcarriers is used, when the correlation is performed over several symbols [3] and when the guard time does not contain much ISI [8].

A method of synchronisation which does not have the drawbacks mentioned above is based on special training symbols. Because the receiver knows the content of these training symbols the entire training signal can be used for synchronisation and not just a small part of each symbol. When the received signal is correlated with the known training signal the resulting signal will contain a peak for each training symbol. Timing can be determined by detecting these peaks and frequency offset can be estimated by looking at the phase of the correlation output, which is equal to the phase drift between samples that are T_s seconds apart. Hence, the frequency offset is equal to the phase of the correlation peak divided by $2\pi T_s$ [3]. According to [9], this method only works for frequency offsets that are smaller than half the training symbol rate. The detection range can be increased by using shorter symbols.

As mentioned before, phase offsets can be estimated and corrected after the FFT by using pilot subcarriers.

3.3 Amplitude Control

When N_s subcarriers are added with the same phase, the resulting signal has a peak power that is N_s times the average power. Hence an OFDM signal can have a large Peak-to-Average Power (PAP) ratio, which is upper limited by the number of subcarriers. A large PAP ratio has several disadvantages, including an increased complexity of the Analogue-to-Digital (ADC) and Digital-to-Analogue Converters (DAC) and a reduced efficiency of the RF power amplifier [3].

To avoid these problems, PAP reduction can be performed by the transmitter. According to [3], this can be done before the IFFT by using special coding or scrambling techniques or after the IFFT by using clipping, peak windowing or peak cancellation. Clipping limits the amplitude to some maximum level. This is the simplest way of PAP reduction but the non-linear distortion of the OFDM signal causes a large amount of out-of-band radiation. Peak windowing causes less out-of-band radiation than clipping as large peaks are multiplied with a certain non-rectangular window. Peak cancellation is a linear PAP reduction

technique and causes almost no out-of-band radiation as large peaks are reduced by subtracting a certain reference signal.
At the receiver the OFDM signal power fluctuates in time due to multipath propagation. To make efficient use of the ADC, the signal power has to be adjusted to the ADC input range by applying Automatic Gain Control (AGC). AGC can be performed by estimating the signal power based on special training symbols, which are transmitted as the initial symbols of a packet [3].

4
IEEE 802.11 Standards

As mentioned in Chapter 1, the IEEE adopted the first standard for WLANs in 1997. This standard, IEEE 802.11, provides reliable data communications at data rates up to 2 Mbps. The standard supports mobility and power savings operations to make optimal use of the advantages of mobile devices. In 1999, the IEEE adopted two extensions to the IEEE 802.11 standard. The first, IEEE 802.11a, uses a complete new physical layer implementations based on OFDM and provides data rates up to 54 Mbps. The second, IEEE 802.11b, is an extension to one of the physical layer implementations of the original standard and provides data rates up to 11 Mbps. This chapter gives an overview of the IEEE 802.11 standards and presents detailed information about the IEEE 802.11a standard.

4.1 IEEE 802.11 Standard

The IEEE 802.11 standard is designed to be indistinguishable from fixed LANs for the higher networks layers. As WLANs differ primarily from wired networks at the PHYsical (PHY) layer and at the Medium Access Control (MAC) sublayer of the Open Systems Interconnection (OSI) reference model, the standard defines both the PHY layer and the MAC sublayer [10], [11].
The IEEE 802.11 standard defines the MAC sublayer and three PHY layers. These are an InfraRed (IR) baseband PHY, a Frequency Hopping Spread Spectrum (FHSS) PHY operation in the 2.4 GHz Industrial, Scientific and Medical (ISM) band and a Direct Sequence Spread Spectrum (DSSS) PHY also operating in the 2.4 GHz ISM band. The IEEE 802.11a standard defines a new PHY based on OFDM operating in the 5 GHz ISM band while the IEEE 802.11b standard extends the DSSS PHY to provide higher data rates. Both extensions use the same MAC sublayer as the IEEE 802.11 standard [11].

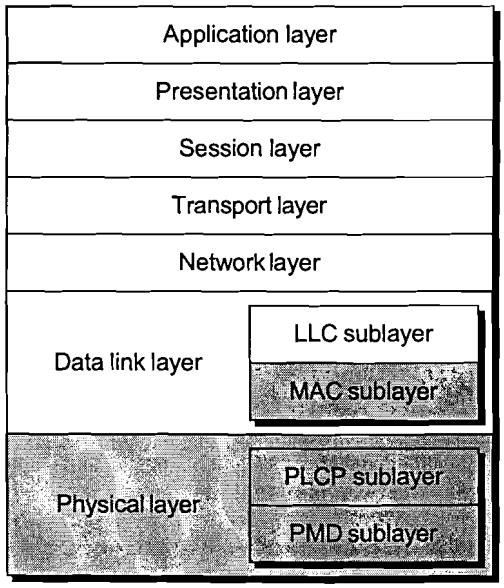

Figure 9: IEEE 802.11 protocol stack and OSI reference model.

The protocol stack of the IEEE 802.11 standard is shown in Figure 9. The MAC sublayer controls the transmission of messages over the wireless medium. The PHY layer is divided in two sublayers. The Physical Layer Convergence Procedure (PLCP) sublayer translates the data received from the MAC into a packet format suitable for the Physical Medium Dependent (PMD) sublayer. The PMD sublayer uses various modulation techniques to transmit these packets over the wireless medium. The focus of this report will be on the implementation of this sublayer. The PMD also provides a carrier sense indication to the MAC. This signal is needed to implement the Carrier Sense Multiple Access with Collision Avoidance (CSMA/CA) protocol used by the IEEE 802.11 standard. With this multiple access protocol, stations sense whether the medium is being used before transmitting to avoid collisions [11].

4.2 IEEE 802.11a Standard

As mentioned before, the IEEE 802.11a defines a new PHY based on OFDM. The standard uses a fixed OFDM symbol length and it defines various coding rates and modulation types for the subcarriers to achieve various data rates. The standard uses a guard time to increase the robustness to delay spread and it uses coding and interleaving to increase the robustness to frequency selective fading and narrow-band interference. Training symbols and pilot subcarriers are used to perform synchronisation at the receiver. Table 1 shows the main parameters of the IEEE 802.11a standard [12].

Table 1: Main parameters.

Property	Value
Symbol duration, T_s	3.2 μs
Subcarrier spacing, f_s	$1/T_s$ = 312.5 kHz
Guard time, T_g	0.8 μs
Total symbol duration, T_{st}	$T_s + T_g$ = 4.0 μs
Symbol rate, r_s	$1/T_{st}$ = 250 ksps
Number of data subcarriers, N_{sd}	48
Number of pilot subcarriers, N_{sp}	4
Total number of subcarriers, N_s	52
Bandwidth	$N_s \times f_s$ = 16.25 MHz

The standard uses either Binary PSK (BPSK), Quadrature PSK (QPSK), 16-QAM or 64-QAM modulation for the subcarriers, depending on the required data rate. BPSK uses the constellation points (-1, 1) and the other modulation schemes use the constellation diagrams shown in Chapter 2, Figure 1. The resulting complex symbols are multiplied by a normalisation factor to achieve the same average power for all constellations. Table 2 shows the various modulation types and data rates [12].

Table 2: Modulation types and data rates.

Modulation type	Normalisation factor	Coding rate	Data rate (Mbps)
BPSK	1	1/2	6
		3/4	9
QPSK	$1/\sqrt{2}$	1/2	12
		3/4	18
16-QAM	$1/\sqrt{10}$	1/2	24
		3/4	36
64-QAM	$1/\sqrt{42}$	2/3	48
		3/4	54

Gray coding is used to map groups of bits to constellation points and vice versa, such that adjacent constellation points differ only by one bit. Gray coding reduces the BER compared to other mapping methods, as only a single bit is corrupted when an adjacent constellation point is erroneously detected by the receiver. At high SNR, this kind of error has a high probability [12].

4.2.1 Transceiver Architecture

Figure 10 shows the general block diagram of an IEEE 802.11a transmitter.

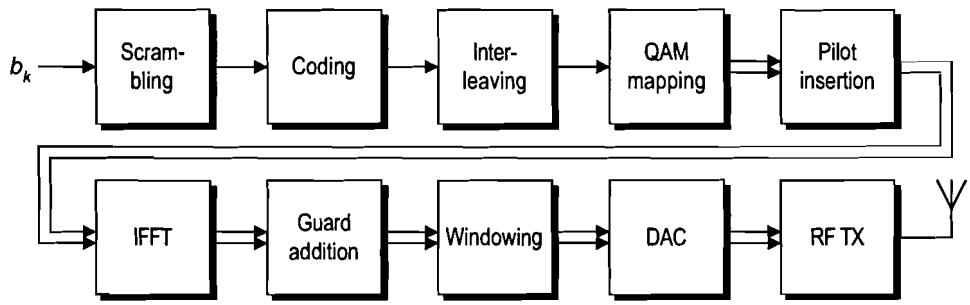

Figure 10: General block diagram of transmitter.

The binary input data symbols b_k are first scrambled to avoid long strings of zeros or ones and then coded by a convolutional encoder with a certain coding rate to enable error recovery at the receiver. The coded bits are interleaved to improve the robustness to burst-errors. The bits are then grouped and mapped to 48 modulation symbols. Four pilot values are added to each group of 48 modulation symbols and all 52 modulation symbols are modulated onto 52 subcarriers by applying the IFFT. The resulting complex baseband signal is equal to the complex envelope of the passband OFDM signal. A guard time is added to improve robustness to delay spread and windowing is applied to reduce the out-of-band spectrum more rapidly. The digital complex baseband signal is converted to an analogue signal by the DAC and subsequently up-converted to the appropriate RF frequency. Finally, the signal is amplified and transmitted through the antenna [3].
Figure 11 shows the general block diagram of an IEEE 802.11a receiver.

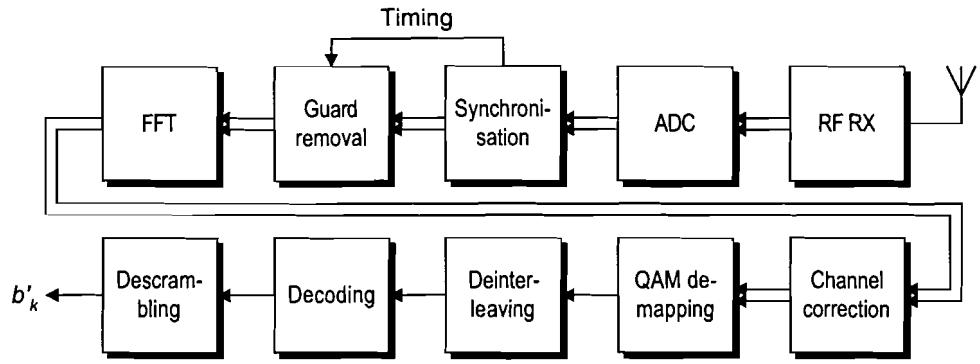

Figure 11: General block diagram of receiver.

The received analogue RF signal is first converted to an analogue complex baseband signal which is equal to the complex envelope of the OFDM signal. This signal is sampled by the ADC. The receiver then performs AGC and estimates the frequency offset and OFDM symbol timing using the special training symbols that are transmitted at the beginning of each OFDM packet. The frequency offset is corrected and, based on the estimated OFDM symbol timing, the guard time is removed. The 52 subcarriers are then demodulated by applying the FFT to recover the 52 modulation symbols. The special training symbols and the pilot values are then used to correct for the channel response and any remaining phase drift before the modulation symbols are demapped into binary data. Finally, the binary data is deinterleaved, decoded and descrambled [3].

4.2.2 Spectral Requirements

As mentioned before, the IEEE 802.11a standard uses the 5 GHz ISM band. Part of the 5 GHz band has been made available for unlicensed use in the United States, Europe and Japan. In the United States, the 5 GHz Unlicensed National Information Infrastructure (U-NII) band is divided in a lower band (5.15-5.25 GHz), a middle band (5.25-5.35 GHz) and an upper band (5.725-5.825 GHz). The lower and upper band contain eight channels spaced 20 MHz apart. There is a space of 30 MHz between the outer channels and the band edges. The upper band contains four channels spaced 20 MHz apart. There is a space of 20 MHz between the outer channels and the band edges. The maximum transmit power is 40 mW for the lower band, 200 mW for the middle band and 800 mW for the upper band. The maximum transmit power level for the lower band is suitable for home and small office environments, while the maximum transmit power level for the upper band is suitable for bridging applications. Hence IEEE 802.11a compliant devices will usually support only some of the frequency bands, depending on their application. In Europe and Japan similar regulations exist [12].

Apart from these regional or national requirements, the IEEE 802.11a standard sets additional requirements regarding the transmitted signal. The transmitted signal spectrum should fall within the transmit spectrum mask, which is shown in Figure 12. Typically, the spectrum has a 3-dB bandwidth of 16.6 MHz. The spectrum should be sufficiently flat, i.e. the average energy of each of the subcarriers –16 to –1 and 1 to 16 should deviate no more than ±2 dB from their average energy and the average energy of each of the subcarriers –26 to –17 and 17 to 26 should deviate no more than +2/–4 dB from the average energy of the subcarriers –16 to –1 and 1 to 16 [12].

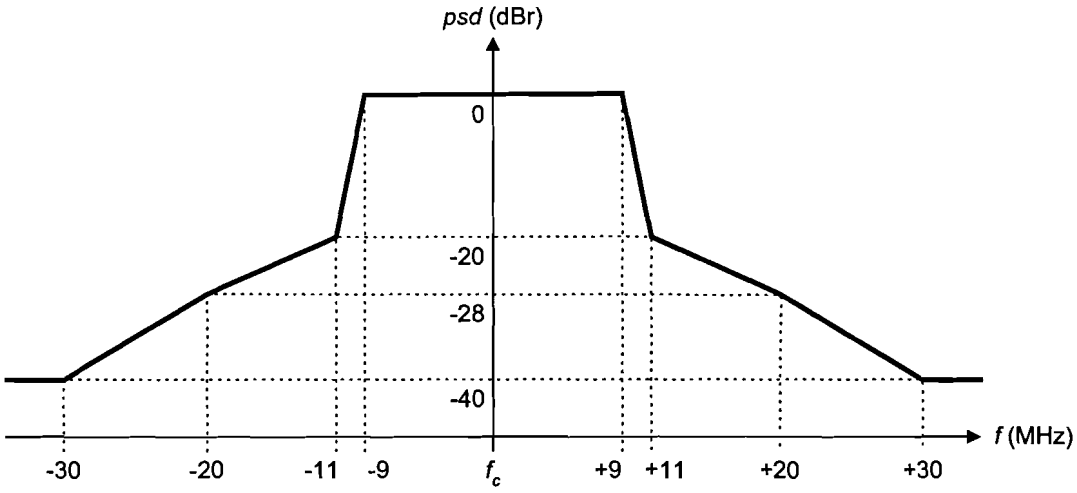

Figure 12: Transmit spectrum mask.

The IEEE 802.11a standard sets requirements for the receiver as well. The minimum sensitivity depends on the data rate and varies from –82 dBm for 6 Mbps to –65 dBm for 54 Mbps, measured at the antenna connector. The maximum input power level is specified as –30 dBm [12].

5
Current Design and Simulation Model of the Baseband Module

As mentioned in Chapter 1, a IEEE 802.11a compliant modem is currently being designed at the Philips Semiconductors Systems Lab Eindhoven. The actual modem implements the OFDM physical layer of the IEEE 802.11a standard and consists of two distinct parts: the digital baseband module and the analogue RF front-end, as illustrated in Figure 13.

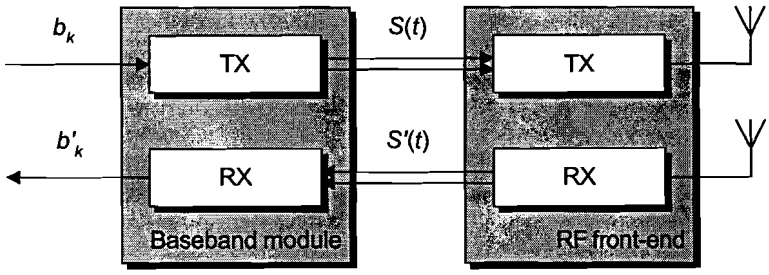

Figure 13: Current transceiver design consists of two parts.

At the transmitter, the baseband module uses the supplied binary data b_k to generate the complex envelope $S(t)$ of the passband OFDM signal and the RF front-end converts the complex envelope to the OFDM signal at the correct RF frequency. Referring to Chapter 4, Figure 10, it can be seen that the baseband module performs all tasks up to and including DAC. At the receiver, the reverse process takes place. The RF front-end retrieves the complex envelope $S'(t)$ of the received OFDM signal and the digital baseband module recovers the transmitted binary data b'_k. Referring to Chapter 4, Figure 11, it can be seen that the baseband module performs all tasks from ADC.
This chapter gives an overview of the tasks performed by the actual baseband module and derives its simulation model. The actual RF front-end and its simulation model are discussed in the next chapter. As mentioned in Chapter 1, a simulation model of the baseband module already exists. The simulation model derived here is a limited model of the baseband module as it is only meant to be a tool for simulations of the RF front-end.

5.1 Transmitter Path

The transmitter path of the actual baseband module performs various tasks to generate the complex envelope of the passband OFDM signal. These tasks and how these are implemented in the simulation model are discussed in the following paragraphs. The simulation model of the transmitter path can be found in Appendix A.

5.1.1 Scrambling, Coding, Interleaving and QAM Mapping

The actual baseband module performs scrambling, coding and interleaving on the binary input data symbols. The resulting binary data symbols are grouped and mapped to modulation symbols. As the binary input data symbols are random, the resulting modulation symbols can be considered to be random. This means that a random PSK or QAM source can be used in the simulation model instead of actually implementing the before mentioned operations.

5.1.2 IFFT and Guard Addition

For each OFDM symbol, the actual baseband module uses a 64-point IFFT to modulate the 52 modulation symbols onto the 52 subcarriers. A 64-point IFFT is used because an N-point IFFT, where N is a power of two, can be efficiently implemented. However, because there are only 52 modulation symbols, zeros have to added to the IFFT input vector. These are added in the middle of the IFFT input vector because the middle elements correspond to the higher positive and negative frequencies, which should not be used.

Referring to Chapter 4, one OFDM symbol must have a duration of 3.2 μs, excluding the guard time. As a 64-point IFFT is used to generate the OFDM symbols, one OFDM symbol consists of 64 samples. This means that the actual baseband module operates at a sample frequency of 64/3.2 μs or 20 MHz.

The actual baseband module adds a guard time to each generated OFDM symbol. Again referring to Chapter 4, the guard time must have a duration of 0.8 μs. As a sampling frequency of 20 MHz is used, the guard time consists of 20 MHz × 0.8 μs or 16 samples.

The simulation model generates the IFFT input vector, performs the IFFT and adds the guard time similar to the actual baseband module, as illustrated in Figure 14.

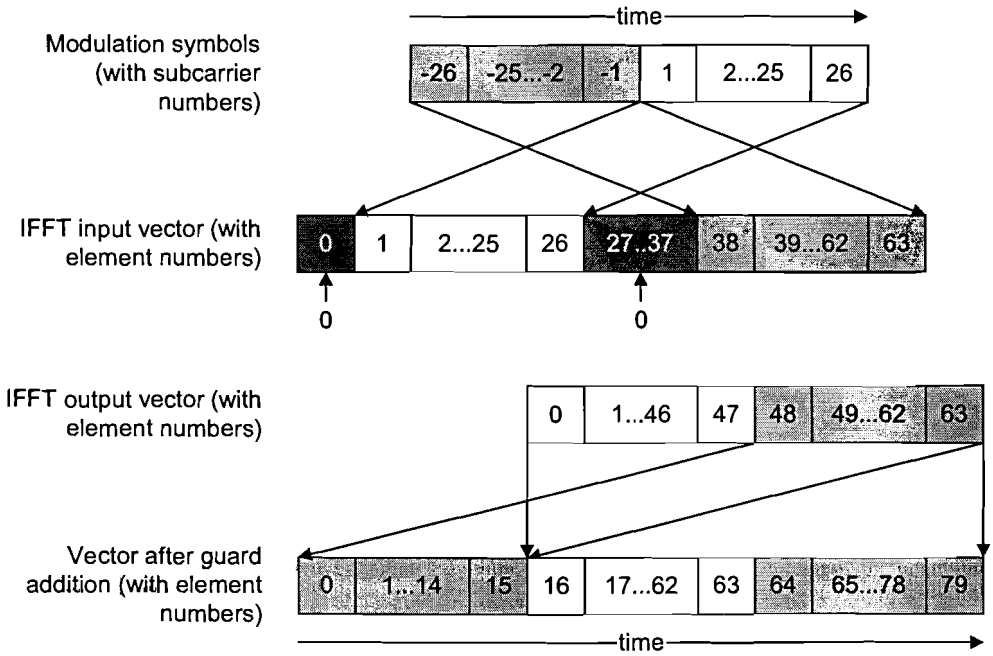

Figure 14: Generation of the IFFT input vector and guard addition.

Using the simulation model, the spectrum of the complex baseband signal after guard addition has been determined, as shown in Figure 15. This figure also shows a detailed view of the spectrum of the main lobe. By looking at the spectrum a few things can be noticed. First of all, the spectrum is periodic with a period of 20 MHz. This is because the sample frequency of the complex baseband signal is 20 MHz. The spectrum consists of distinct peaks. This is because the complex baseband signal consists of 52 subcarriers with their own distinct frequency. As the subcarriers are spaced at 312.5 kHz, the main lobe has a bandwidth of 52 × 312.5 kHz or 16.25 MHz. No subcarrier is present at the centre frequency because the 0th IFFT input is not used.

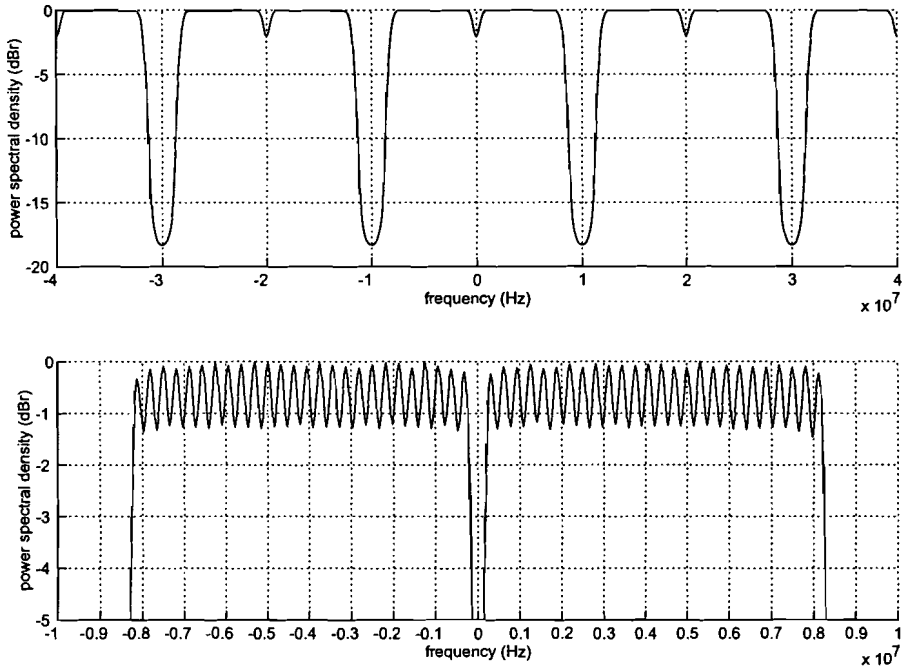

Figure 15: Spectrum of simulated complex baseband signal after guard addition.

It should be noted that plots generated by simulations are always influenced by the simulation parameters and the methods used to generate the plot from the simulation data. For example, the simulation sampling frequency f_s limits the frequency range of spectrum plots from $-f_s/2$ to $+f_s/2$. As another example, the number of points used to generate a plot limits the amount of detail that can be seen in the plot. This should be taken into account when interpreting simulation results.

5.1.3 Windowing

It was mentioned in Chapter 3 that windowing can be used to reduce the out-of-band spectrum. However, in the actual baseband module, windowing is not performed for two reasons. First of all, windowing is not easy to implement because the OFDM symbols need to be extended and concatenated. Second, it was thought by the designers of the actual baseband module that the amount of out-of-band spectrum was low enough to comply to the spectral requirements of the IEEE 802.11a standard, either directly or after filtering. As windowing is not

performed by the actual baseband module, it is not performed by the simulation model.

5.1.4 Digital-to-Analogue Conversion

The DACs convert the digital, sampled complex baseband signal to an analogue, continuous complex baseband signal. The simulation model can model the DACs using a sample-and-hold block and by converting from fixed point to floating point. However, the system will first be modelled in floating point. The effects of fixed point can be considered later. The sample-and-hold block actually repeats any sample for a number of simulation cycles and thus increases the sampling frequency of the complex baseband signal.

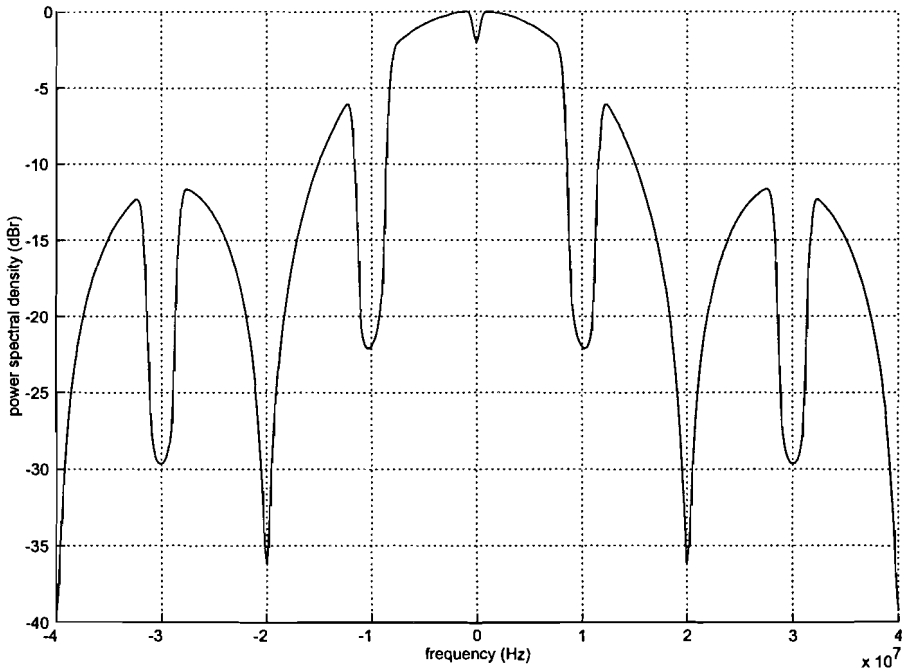

Figure 16: Spectrum of simulated complex baseband signal after DAC.

Using the simulation model, the spectrum of the complex baseband signal after the DAC has been determined, as shown in Figure 16. A few things can be noticed from the above figure. It can be seen that the spectrum is a combination of the spectrum of the complex baseband signal and the sinc-like frequency response of the sample-and-hold block. This causes the roll-off of the main lobe and the relatively high power of the first side lobes. This will make it harder to satisfy the spectral requirements of the IEEE 802.11a standard, as explained in Chapter 4. However, an analogue Low-Pass Filter (LPF) can be used after the DAC to reduce the power of the side lobes. As the side lobes are close to the main lobe and have relatively high power, the analogue filter must have a fast transition from passband to stopband. Such a filter might be difficult to implement.

5.1.5 Sample Rate Conversion

To reduce the demands placed on the analogue low-pass filter, the designers of the actual baseband module decided to operate the DAC at the higher sampling rate of 40 MHz. When a higher sampling rate is used, the side lobes will be

moved further away from the main lobe, which means that the analogue low-pass filter can have a slower transition from passband to stopband. Additionally, the roll-off is reduced because the main lobe of the sample-and-hold spectrum will be wider at this higher sampling rate.
To obtain this higher sampling rate a sample rate converter is needed, which consists of an upsampler followed by a digital low-pass interpolation filter. The actual baseband module uses a linear phase FIR filter in order to avoid phase rotations. The passband of the filter ranges from DC to 8.3 MHz, which is half of the 3-dB bandwidth of the OFDM signal, referring to Chapter 4. The stopband of the filter starts at 20 – 8.3 MHz or 11.7 MHz, where the first side lobe begins [13]. Using the SPW Filter Design System (FDS), a filter was designed which matches the actual interpolation filter as good as possible. This filter is used by the simulation model and its frequency response is shown in Figure 17.

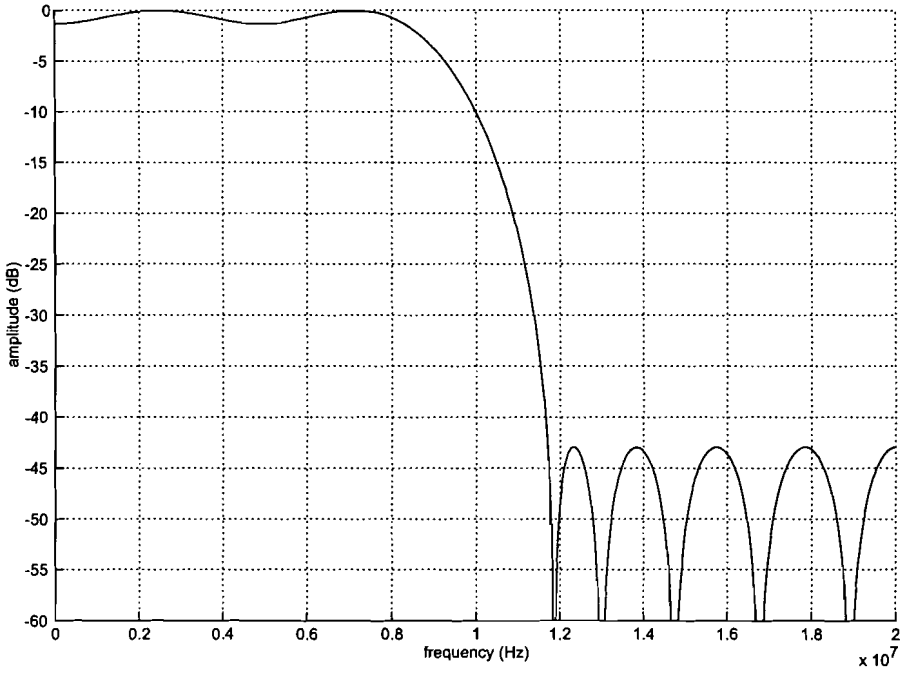

Figure 17: Interpolation filter used for simulations.

Using the simulation model, the spectrum of the complex baseband signal after the sample rate conversion and DAC has been determined as shown in Figure 18. A few things can be noticed when comparing the spectra of the complex baseband signal with and without sample rate conversion. The first side lobe is moved further away from the main lobe, which reduces the demands placed on the analogue low-pass filter. However, the filter is still needed to reduce the power of the remaining side lobes. The roll-off of the main lobe is reduced but the interpolation filter introduces ripples in the spectrum of the complex baseband signal as its frequency response is not flat in the passband. To verify that the spectral flatness requirements of the IEEE 802.11a standard are met, a detailed view of the main lobe is shown in Figure 19. It can be seen that the spectral flatness is still within the limits set by the IEEE 802.11a standard.

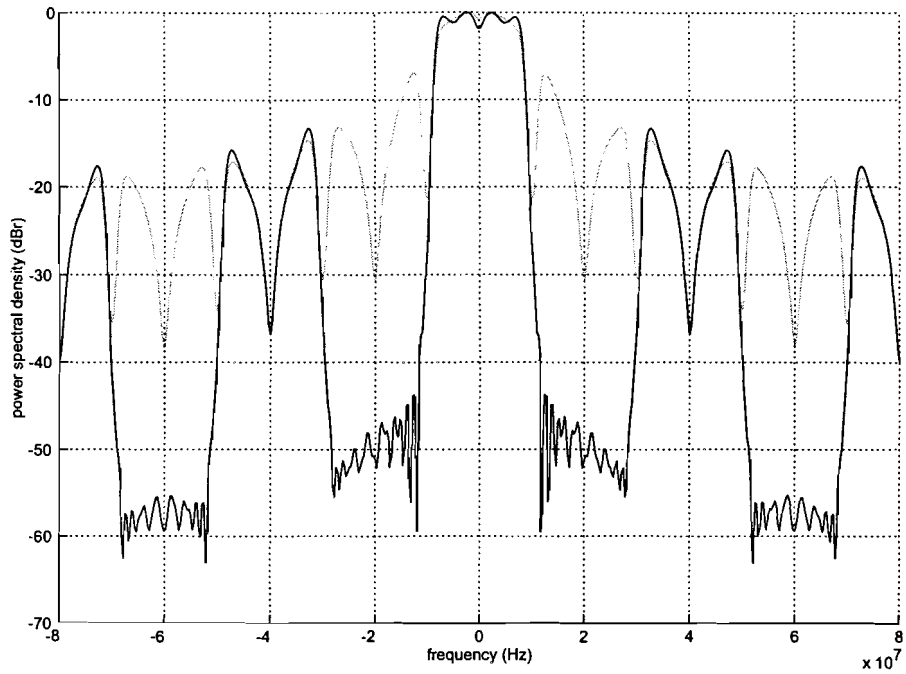

Figure 18: Spectrum of simulated complex baseband signal after sample rate conversion and DAC. The spectrum without sample rate conversion is also shown for comparison.

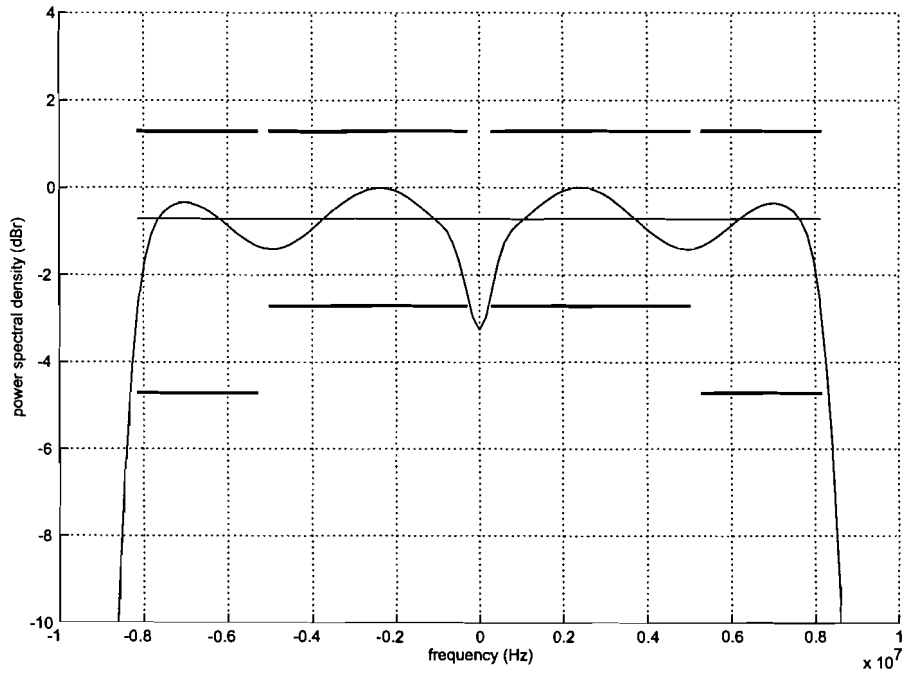

Figure 19: Detail of the spectrum of the simulated complex baseband signal after sample rate conversion and DAC. The bold lines represent the spectral flatness limits.

5.2 Receiver Path

The receiver path of the actual baseband module performs various tasks to recover the transmitter binary data. These tasks and how these are implemented

in the simulation model are discussed in the following paragraphs. The simulation model of the receiver path can be found in Appendix A.

5.2.1 Analogue-to-Digital Conversion

The actual baseband module uses an ADC to convert the analogue, continuous complex baseband signal to a digital, sampled complex baseband signal. The simulation model can model the ADC using a downsampling block and by converting from floating point to fixed point. As mentioned before, the system will first be modelled in floating point and the effects of fixed point can be considered later.

5.2.2 Synchronisation, Guard Removal and FFT

The actual baseband module uses training symbols to determine symbol timing, as explained in Chapter 3 and Chapter 4. Based on the detected symbol timing, the 16 sample guard time is removed and the remaining 64 samples are used as the input vector to the FFT. From the 64-element FFT output vector, the 52 non-zero elements are converted to consecutive modulation symbols.
The simulation model performs guard removal and the FFT similar to the actual baseband module but does not perform symbol timing based on training symbols. This approach is chosen to limit the complexity of the simulation model.
Chapter 3 explained that symbol timing based on training symbols is done by correlating the received signal with the known training signal. In the simulation model, a similar approach can be used as the transmitted signal is known. By correlating the transmitted signal, which is the output signal of the simulation model of the transmitter path, and the received signal, which is the input signal to the simulation model of the receiver path, the delay can be determined by detecting the peak in the correlation output. If the delay is n samples, the correlation peak will be shifted by n samples from the correlation output centre. Synchronisation is achieved by discarding the first n samples of the received signal before it is further processed by the simulation model of the receiver path. Synchronisation is also achieved if an additional delay is introduced, such that the total delay is as long as an integer number of OFDM symbols. As this method is more efficient in terms of simulation time, this is the method used in the simulation model. The simulation model of the synchronisation block can be found in Appendix A.

5.2.3 Channel Correction, QAM Demapping, Deinterleaving, Decoding and Descrambling

The actual baseband module performs channel correction, QAM demapping, deinterleaving, decoding and descrambling to retrieve the transmitted binary data symbols. All these tasks are not performed by the simulation model to limit the complexity of the model.
To verify the simulation model of the baseband module, the complex baseband signal generated by the simulation model of the transmitter path has been applied to the simulation model of the receiver path. Symbol timing has been performed as described in the previous paragraph. The transmitted and received constellation diagrams are shown in Figure 20.

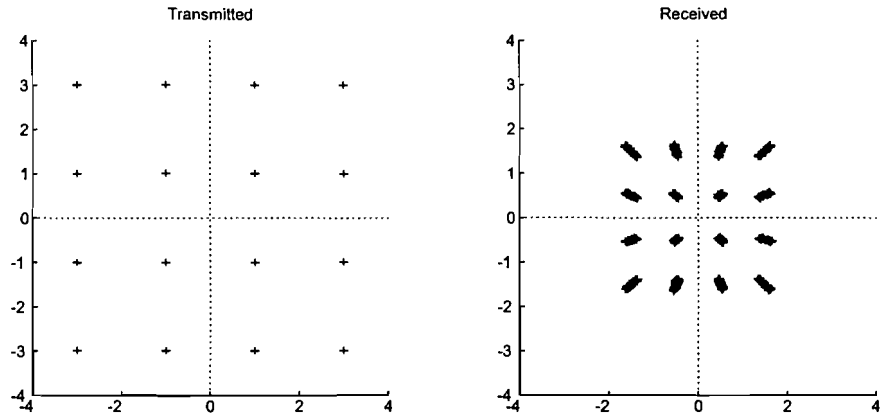

Figure 20: Simulated transmitted and received constellation diagrams.

The above figure shows all transmitted and received modulation symbols from all subcarriers. It is clear that the phase of the modulation symbols is not affected and that the amplitude is effected with variable attenuation. The phase is not effected because there are no blocks in the simulation model that introduce a phase rotation. Phase rotations are often introduced by non-linear phase filters but the used interpolation filter is a linear phase filter. The amplitude is affected with variable attenuation because the frequency response of the used interpolation filter is not flat in the passband. The attenuation of the modulation symbols depends on the attenuation of the subcarrier on which they are modulated. While the attenuation varies between subcarriers, the attenuation for each subcarrier is constant.

6
Current Design and Simulation Model of the RF Front-end

As mentioned before, the actual RF front-end converts the complex envelope of the passband OFDM signal to the OFDM signal at the correct RF at the transmitter and retrieves the complex envelope of the received OFDM signal at the receiver. The RF front-end performs these conversions using an Intermediate Frequency (IF) of 1.489 GHz. Many transceivers use an IF as signal processing, e.g. filtering and amplification, can be performed easier at the lower IF frequencies than at the high RF frequencies.
The actual RF front-end generates carrier signals and passband signals at high frequencies compared to the bandwidth of the OFDM signal. Generating these high frequency signals would require a high sampling rate for the simulation model, which would result in low simulation speeds. For this reason, the simulation model uses a different approach: it uses the complex envelope to represent all passband signals. As the bandwidth of the complex envelope is much smaller than the frequencies of the high frequency signals the sampling frequency can be reduced which increases simulation speed. An example can illustrate this. Consider a passband signal with a bandwidth of 20 MHz at 5 GHz. Simulation of the passband signal requires a sampling rate of at least twice the maximum frequency or 10 GHz. Simulation of the complex envelope requires a simulation sampling rate of at least 20 MHz. Hence when the complex envelope is used to represent the passband signal the simulation speed is increased by a factor $10 \cdot 10^9 / 20 \cdot 10^6$ or 500.
This chapter discusses the actual RF front-end. It describes the function of the various components and describes the effect of imperfections of the components. For each component a simulation model is derived.

6.1 Transmitter Path

The transmitter path of the actual RF front-end consists of two stages. The first stage, which converts the complex envelope of the passband OFDM signal to the OFDM signal at the IF, is implemented as a single Integrated Circuit (IC), the SA5730. The second stage, which converts the OFDM signal from the IF to the RF, uses an IC, the SA5710, and additional filters and amplifiers. Both ICs are specifically designed for this application. Figure 21 shows the basic building blocks of the transmitter path of the actual RF front-end. The in-phase signal $I(t)$ and the quadrature signal $Q(t)$ are the real and imaginary parts of the complex envelope $S(t) = I(t) + jQ(t)$ of the passband OFDM signal received from the baseband module.

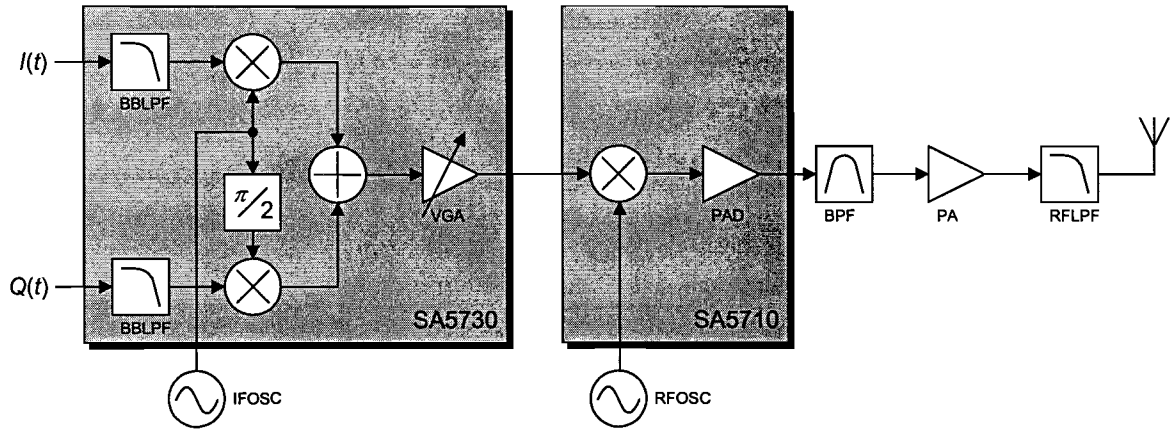

Figure 21: Transmitter path of the actual RF front-end.

The following paragraphs describe the various building blocks of the transmitter path in more detail.

6.1.1 Baseband Low-pass Filters

The baseband low-pass filters of the actual RF front-end pass the main lobe of the OFDM signal and filter out the side lobes. For the simulation model, a filter has been designed using FDS, which matches the actual baseband low-pass filter [14] as good as possible. The simulation model filter is a third order, Elliptic low-pass filter. The frequency response of the simulation model filter can be found in Appendix B.

The simulation model uses a single filter block to filter the complex baseband signal. This implies that the in-phase and quadrature signals are filtered by identical filters. In practice, this is not achievable as there will always be a certain mismatch between both filters. The simulation model can be modified to use two separate filter blocks if more data on the actual filters becomes available.

6.1.2 Quadrature Modulator

The quadrature modulator of the actual RF front-end modulates the in-phase signal $I(t)$ by the oscillator signal and the quadrature signal $Q(t)$ by the $\pi/2$ phase-shifted oscillator signal. The oscillator is set to a fixed frequency equal to the IF frequency ω_{IF}. Both modulated signals are summed, which results in the real-valued passband signal given by

$$\begin{aligned} s(t) &= I(t)\cos(\omega_{IF}t) - Q(t)\sin(\omega_{IF}t) \\ &= \mathrm{Re}\left\{\left[I(t) + jQ(t)\right]e^{j\omega_{IF}t}\right\} \\ &= \mathrm{Re}\left\{S(t)e^{j\omega_{IF}t}\right\} \end{aligned} \tag{8}$$

This equation shows that the quadrature modulator output is the real part of the complex baseband signal $S(t)$, multiplied by the complex carrier $\exp(j\omega_{IF}t)$. Multiplication by the complex carrier $\exp(j\omega_{IF}t)$ shifts the signal spectrum by the carrier frequency. Taking the real part results in a symmetrical spectrum. The spectra of the complex baseband signal and the quadrature modulated signal are illustrated in Figure 22.

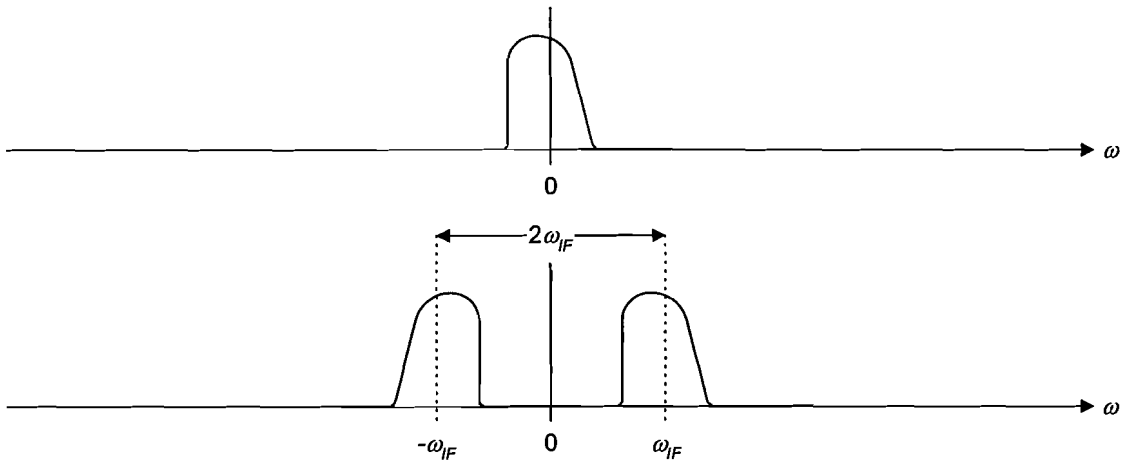

Figure 22: Simplified spectra of the input signal and the output signal of the actual quadrature modulator.

Equation (8) shows that the complex envelope of the passband signal $s(t)$ is equal to the complex baseband signal $S(t)$. As the simulation model uses the complex envelope to represent passband signals, this would mean that the quadrature modulator does not need to be included in the simulation model. However, practical quadrature modulators suffer from various non-idealities, which deform the complex envelope of the passband signal. These non-idealities include gain and phase imbalance, phase noise and frequency error.

Gain and *phase imbalance* can occur when the in-phase and quadrature signals are separately converted, amplified or filtered. The quadrature modulator output in the case of gain and phase imbalance is given by

$$s(t) = I(t)\cos(\omega_{IF}t) - g_e Q(t)\sin(\omega_{IF}t + \varphi_e) \tag{9}$$

In this equation, the in-phase signal is chosen as the reference and g_e and φ_e are the gain and phase of the quadrature signal relative to the in-phase signal. Equation (9) can be rewritten as

$$\begin{aligned} s(t) &= \{I(t) - g_e Q(t)\sin(\varphi_e)\}\cos(\omega_{IF}t) - \{g_e Q(t)\cos(\varphi_e)\}\sin(\omega_{IF}t) \\ &= I'(t)\cos(\omega_{IF}t) - Q'(t)\sin(\omega_{IF}t) \end{aligned} \tag{10}$$

This equation shows that the complex envelope of the quadrature modulated signal, in the case of gain and phase imbalance, is given by $I'(t) + jQ'(t)$ [15].

Phase noise has already been discussed in Chapter 3. Given a phase noise signal $\varphi_n(t)$, the complex envelope of the quadrature modulated signal is equal to [16]

$$S(t) = \{I(t) + jQ(t)\}e^{j\varphi_n(t)} \tag{11}$$

A *frequency error* occurs when the oscillator frequency is not correctly set. As a result, the signal spectrum is not shifted to the correct frequency. The complex envelope of the quadrature modulated signal including a frequency error of ω_e is given by [16]

$$S(t) = \{I(t) + jQ(t)\}e^{j\omega_e t} \tag{12}$$

Practical quadrature modulators do not actually perform the multiplication of the input signal by the carrier signal, as expressed in equation (8). Instead, they use a switching circuit that switches the input signal phase by 180° every time the

carrier signal changes polarity. This can be seen as multiplying the input signal by a square wave with unit amplitude and a frequency equal to the carrier frequency. The switching circuit consists of either diodes or transistors. As these are non-linear devices, practical quadrature modulators introduce non-linear distortion. When diodes are used, which are passive devices, the power of the output signal will be less than the power of the input signal and the quadrature modulator introduces conversions loss. When transistors are used, which are active devices, the quadrature modulator introduces conversion gain. As the specifications of the SA5730 [14] only specify the gain and non-linear behaviour of the entire IC, the gain and non-linearity of the quadrature modulator itself are not known. The simulation model uses a linear model with unit gain for the quadrature modulator and uses a non-linear model for the amplifier of the SA5730 to account for the gain and non-linearities of the entire IC.
The simulation model of the quadrature modulator uses equations (10), (11) and (12) to generate the complex envelope of the quadrature modulated signal including gain and phase imbalance, phase noise and frequency error. The simulation model of the quadrature modulator can be found in Appendix A.

6.1.3 IF Oscillator

The IF oscillator of the actual RF front-end generates the carrier signal for the quadrature modulator. As the simulation model uses the complex envelope to represent signals, no carrier signal needs to be calculated and the oscillator does not need to be included in the simulation model. Practical oscillators, however, suffer from *phase noise*, which deforms the complex envelope of the quadrature modulated signal.
Referring to Chapter 3, the PSD of the phase noise signal $\varphi_n(t)$ is given by

$$\Phi_n(f) = \frac{K}{\pi\beta}\frac{1}{1+(f/\beta)^2} = \frac{K}{\pi\beta}|H(f)|^2 \tag{13}$$

In this equation, $H(f)$ is equal to the frequency response of a first order, Butterworth low-pass filter with a cut-off frequency of β. The factor $K/\pi\beta$ can be interpreted as the PSD of a white noise signal. Hence the phase noise signal can be generated by filtering a white noise signal with the given Butterworth filter. As the PSD of the white noise signal is given by $K/\pi\beta$, the power is given by $Kf_s/\pi\beta$, where f_s is the simulation sampling frequency. The simulation model of the oscillator, which can be found in Appendix A, uses this method to generate the phase noise signal. In the simulation model, the total integrated phase noise power K is specified directly, while the 3-dB linewidth is based on the value of the specified power spectral density at the specified frequency. The simulation model parameters are based on the specifications [14], which are not reprinted here because of confidentiality.

6.1.4 Variable Gain Amplifier

The Variable Gain Amplifier (VGA) of the actual RF front-end attenuates or amplifies the signal. The gain can be set to a specific level, which is used to control the transmitter output power.
Practical amplifiers are *non-linear devices*, whose transfer function is not constant but a function of the input (or output) signal. For solid-state amplifiers,

this usually means that the gain of the amplifier is a function of the amplitude of the input signal. Non-linearities cause saturation, harmonics and intermodulation.
If the amplitude of the input signal is low, the amplifier operates in the linear region and the gain is approximately constant. If the input signal amplitude increases, the gain decreases and the amplitude of the output signal will approach the saturation amplitude. In the non-linear region, the complex envelope of the input signal is distorted. This is a problem for linear modulation techniques, such as OFDM, where the information is incorporated in the signal amplitude. When a linear modulation technique is used, amplifiers should be used primarily in the linear region [3].
If the input signal contains only one frequency, the output signal of a non-linear amplifier will not only contain the input frequency but also harmonics of this frequency. The harmonics do not interfere with the original signal as they are located at out-of-band frequencies. They are usually filtered out to reduce interference to other systems. However, if the input signal contains multiple frequencies, such as an OFDM signal, the output signal does not only contain the input frequencies and their harmonics but also their sum and difference frequencies. These are called intermodulation products and some of these intermodulation products interfere with the original signal as they are located in-band and cannot be filtered out. As the amplitudes of the intermodulation products increase near saturation, a certain back-off is needed to reduce intermodulation interference [5], [17], [18].
A non-linear amplifier is often modelled using a polynomial. Even-order terms are usually not included as they do not result in any in-band interference; odd-order terms with order higher than three are usually not included as they result in interference with negligible power with respect to interference caused by the third-order term [5], [17], [18]. Hence the non-linear amplifier response is given by

$$y(t) = G\left\{x(t) - \alpha x^3(t)\right\} \tag{14}$$

In equation (14), G is the small signal gain and α determines the non-linear characteristics of the amplifier. The equation is valid if $x(t)$ is smaller than the saturation input given by

$$\begin{aligned} \left.\frac{dy}{dx}\right|_{x=x_{sat}} &= 0 \\ x_{sat} &= \sqrt{\frac{1}{3\alpha}} \end{aligned} \tag{15}$$

In practice, the non-linearity of the amplifier is specified by the 1-dB Compression Point (CP) or the third order Intercept Point (IP3). The value of α can be related to the CP by looking at the amplifier response to a single, sinusoidal input:

$$\begin{aligned} x(t) &= A\cos(\omega t) \\ y(t) &= \left\{GA - \frac{3}{4}\alpha G A^3\right\}\cos(\omega t) - \frac{1}{4}\alpha G A^3 \cos(3\omega t) \end{aligned} \tag{16}$$

The input-referred CP (ICP) is defined as the value of the sinusoidal input, for which the amplitude of the first-order term is 1 dB below the amplitude of the output, if a linear amplifier was used [5], [18]:

$$20\log\left\{G\cdot ICP-\frac{3}{4}\alpha G\cdot ICP^3\right\}=20\log(G\cdot ICP)-1$$
$$\alpha=\frac{4(1-10^{-1/20})}{3\cdot ICP^2} \tag{17}$$

The value of α can be related to the IP3 by looking at the amplifier response to two sinusoidal inputs with distinct frequencies ω_1 and ω_2:

$$\begin{aligned}x(t)&=A\{\cos(\omega_1 t)+\cos(\omega_2 t)\}\\ y(t)&=\left\{GA-\frac{9}{4}\alpha GA^3\right\}\{\cos(\omega_1 t)+\cos(\omega_2 t)\}\\ &-\frac{1}{4}\alpha GA^3\{\cos(3\omega_1 t)+\cos(3\omega_2 t)\}\\ &-\frac{3}{4}\alpha GA^3\{\cos(2\omega_1 t-\omega_2 t)+\cos(2\omega_2 t-\omega_1 t)+\cos(2\omega_1 t+\omega_2 t)+\cos(2\omega_2 t+\omega_1 t)\}\end{aligned} \tag{18}$$

This equation shows that the output contains the fundamental frequencies ω_1 and ω_2, the third order harmonic frequencies $3\omega_1$ and $3\omega_2$ and the intermodulation products. Based on the intermodulation products, the input-referred IP3 (IIP3) is defined as the value of the amplitude of the sinusoidal inputs, for which the amplitude of the intermodulation terms equals the amplitude of the output, if a linear amplifier was used [5]:

$$\frac{3}{4}\alpha G\cdot IIP3^3=G\cdot IIP3$$
$$\alpha=\frac{4}{3\cdot IIP3^2} \tag{19}$$

According to equations (17) and (19), there is a strict relationship between ICP and IIP3, which is given by

$$IIP3=ICP+9.6\text{ dB} \tag{20}$$

According to [5], this strict relationship between ICP and IIP3 does not hold for practical non-linear amplifiers as they do not only present first- and third-order non-linearity but also higher order non-linearity. Hence for practical amplifiers the value of α as a function of the specified ICP will, in general, differ from the value of α as a function of the IIP3. This means that two different amplifier models exist for a single practical amplifier. As the IIP3 is related to intermodulation, it can be expected that the amplifier model based on the IIP3 will model distortion caused by intermodulation accurately. As the ICP is related to saturation, it can be expected that the amplifier model based on the ICP will model distortion caused by saturation accurately. However, distortion caused by saturation can be limited if the amplifier is used primarily in the linear region, whereas distortion caused by intermodulation is always present. Because of this, it is advisable to base the model on the IIP3.

Equation (14) described the amplifier response, where both the input signal and the output signal were practical, real-valued signals. The simulation model, however, uses the complex envelope to represent signals. Hence equation (14) cannot be used in the simulation model to model the amplifier. An equation needs to be found that describes the amplifier response, where both the input signal and the output signal are represented by their complex envelope. Such an equation can be found by looking at the amplifier response to a quadrature modulated signal:

$$\begin{aligned} x(t) &= I(t)\cos(\omega t) - Q(t)\sin(\omega t) \\ y(t) &= G\left\{I(t) - \frac{3}{4}\alpha I^3(t) - \frac{3}{4}\alpha I(t)Q^2(t)\right\}\cos(\omega t) \\ &\quad - G\left\{Q(t) - \frac{3}{4}\alpha Q^3(t) - \frac{3}{4}\alpha I^2(t)Q(t)\right\}\sin(\omega t) \\ &= I'(t)\cos(\omega t) - Q'(t)\sin(\omega t) \end{aligned} \tag{21}$$

Calculating the amplifier response involves standard trigonometric identities and during the calculations, higher order harmonics are ignored as they are out of band. Refer to Appendix C for the calculation of the amplifier response. Equation (21) shows that the complex envelope of the amplifier response to an input signal with complex envelope $I(t) + jQ(t)$ is given by $I'(t) + jQ'(t)$.
The simulation model of the VGA uses the result from equation (21) to calculate the complex envelope of the output signal, given the complex envelope of the input signal. The input signal is clipped on the amplitude at x_{sat}. The simulation model of the non-linear amplifier can be found in Appendix A. The simulation model parameters are based on the specifications [14], which are not reprinted here because of confidentiality.

6.1.5 Mixer

The mixer of the actual RF front-end multiplies the quadrature modulated signal with the oscillator signal. The oscillator is set to a variable frequency ω_m. The resulting signal $s_m(t)$ is given by

$$\begin{aligned} s_m(t) &= s(t)\cos(\omega_m t) \\ &= \frac{1}{2}s(t)\left\{e^{j\omega_m t} + e^{-j\omega_m t}\right\} \end{aligned} \tag{22}$$

This equation shows that the mixer output is equal to the input signal, multiplied by the complex carriers $\exp(j\omega_m t)$ and $\exp(-j\omega_m t)$. Multiplication by the complex carriers shifts the spectrum by the positive and negative carrier frequency, as illustrated in Figure 23.

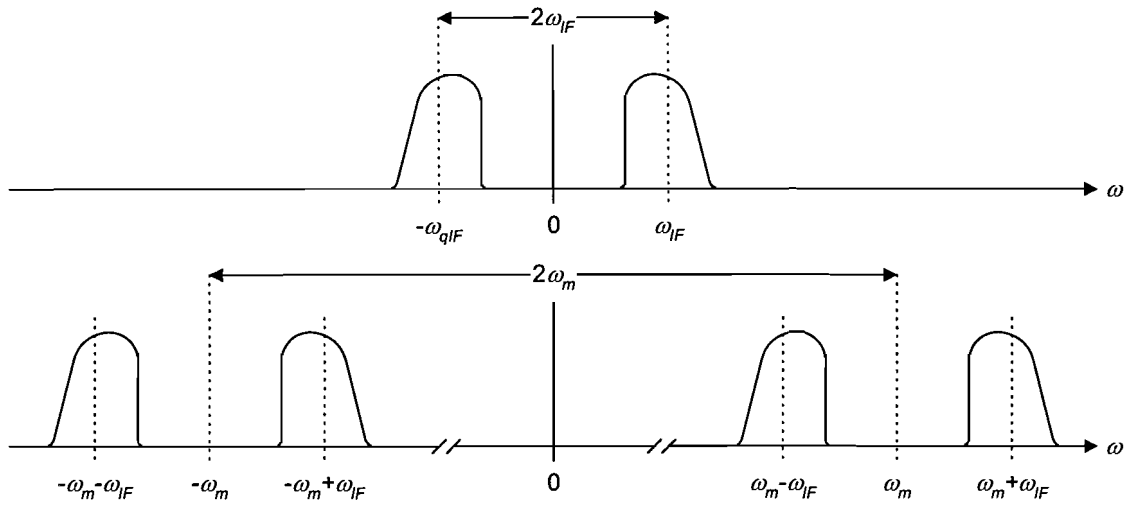

Figure 23: Simplified spectra of the input signal and the output signal of the actual mixer.

As can be seen in Figure 23, the mixer output signal contains two spectral components. Either one is transmitted and the other needs to be filtered out after the mixer. In the actual RF front-end, the spectral component centred at $\omega_m - \omega_{IF}$ is transmitted. This component should be centred at ω_{RF}, the RF frequency of the wanted channel in the 5 GHz ISM band. Hence the oscillator frequency ω_m of the mixer should be set to $\omega_{RF} + \omega_{IF}$.

The complex envelope of the passband signal is not changed by the mixer. As the simulation model uses the complex envelope to represent passband signals, this would mean that the mixer does not need to be included in the simulation model. However, practical mixers suffer from various non-idealities, which deform the complex envelope of the passband signal. Mixers suffer from *phase noise* and *frequency error* but do not suffer from gain and phase imbalance, as the mixer acts on the quadrature modulated signal and not on the in-phase and quadrature signals separately.

Just like practical quadrature modulators, practical mixers introduce non-linear distortion and conversion gain or loss. As the specifications of the SA5710 [19] only specify the gain and the non-linear behaviour of the entire IC, the gain and non-linearity of the mixer itself are not known. The simulation model uses a linear model with unit gain for the mixer and uses a non-linear model for the amplifier of the SA5710 to account for the gain and the non-linearities of the entire IC.

The simulation model of the mixer uses equations (11) and (12) to generate the complex envelope of the mixed signal including phase noise and frequency error. The simulation model of the mixer can be found in Appendix A.

6.1.6 RF Oscillator

The RF oscillator of the actual RF front-end generates the carrier signal for the mixer. The simulation model of this oscillator is equal to the simulation model of the first oscillator. As no specifications of the RF oscillator are available, the simulation model will use the same parameters as the IF oscillator.

6.1.7 Power Amplifier Driver

The Power Amplifier Driver (PAD) of the actual RF front-end amplifies the signal to achieve enough power at the Power Amplifier (PA) input. The simulation model of the PAD is equal to the simulation model of the VGA. The simulation model parameters are based on the specifications [19], which are not reprinted here because of confidentiality.

6.1.8 Band-pass Filter

The main function of the Band-Pass Filter (BPF) of the actual RF front-end is to filter out the spectral component located at the image frequency $\omega_{RF} + 2\omega_{IF}$. It should pass all frequencies inside the 5 GHz ISM band with low distortion. For the United States, Figure 24 shows the location of the 5 GHz U-NII band, the image frequencies and the general shape of the band-pass filter frequency response.

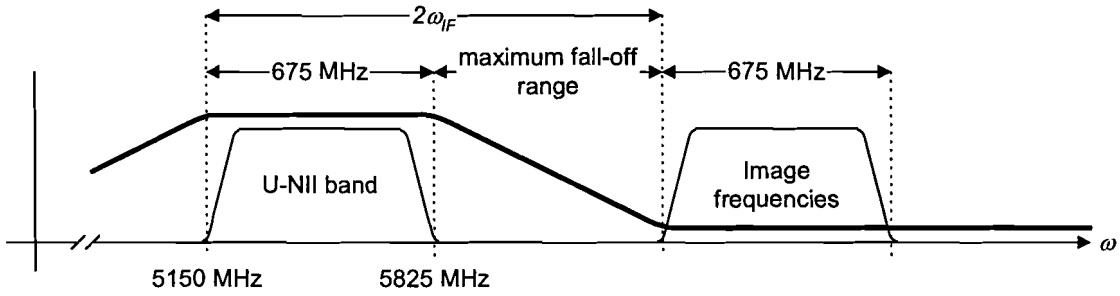

Figure 24: U-NII band, image frequencies and band-pass filter frequency response (bold line).

As can be seen from the above figure, the distance between the U-NII band frequencies and image frequencies is determined by the IF. As the filter must pass the U-NII band frequencies and should filter out the image frequencies, the maximum fall-off range is determined by the IF. In practical filters, there is usually a trade-off between the fall-off rate and the spectral flatness or linear phase in the passband. If the IF is chosen large enough, the fall-off rate can be chosen to be low, which allows the filter to have good passband properties.
As only limited specifications of the band-pass filter are available, the simulation model of the band-pass filter consists of an attenuator with an attenuation of 1 dB.

6.1.9 Power Amplifier

The PA of the actual RF front-end amplifies the signal to the correct transmit power level. As mentioned before, the VGA is used to control the transmit power level, as the PA has a fixed gain. The simulation model of the PA is equal to the simulation model of the VGA. Table 3 shows the specifications [20] and the simulation model parameters. The simulation model parameters are based on the specifications, unless otherwise stated.

Table 3: PA specifications and simulation model parameters.

Specifications		
Gain	At the CP, at 5.2 GHz At the CP, at 5.5 GHz At the CP, at 5.8 GHz	29.5 dB 26.5 dB 26.5 dB
Output referred CP		22.5 dBm
Maximum input power		7 dBm
Simulation model parameters		
Gain G	Average value	29 dB
Input referred CP ICP	Average value	–5.5 dBm
Model based on		Compression point
Noise figure F	Not specified, set to zero	0 dB

6.1.10 RF Low-pass Filter

The RF low-pass filter of the actual RF front-end passes all frequencies inside the 5 GHz ISM band and filters out harmonics generated by the PA. As the first harmonic is located at twice the RF frequency, the fall-off of the low-pass filter is directly determined by the RF frequency.
As no specifications of the RF low-pass filter are available, the simulation model of the RF low-pass filter consists of an attenuator with an attenuation of 1 dB.

6.1.11 Antenna

The antenna of the actual RF front-end transmits the signal. As no specifications of the antenna are available, the simulation model of the antenna consists of an amplifier with a typical gain of 0 dB.

6.1.12 Power Distribution

The specifications of the SA5730 [14] specify the typical output power as –20 dBm. This is used as the reference for the power distribution calculation shown in Figure 25. Assuming that typical operation implies maximum transmit power at the antenna, the output power of the SA5730 is –20 dBm for a maximum VGA gain of 0 dB and –41 dBm for a minimum VGA gain of –21 dB.

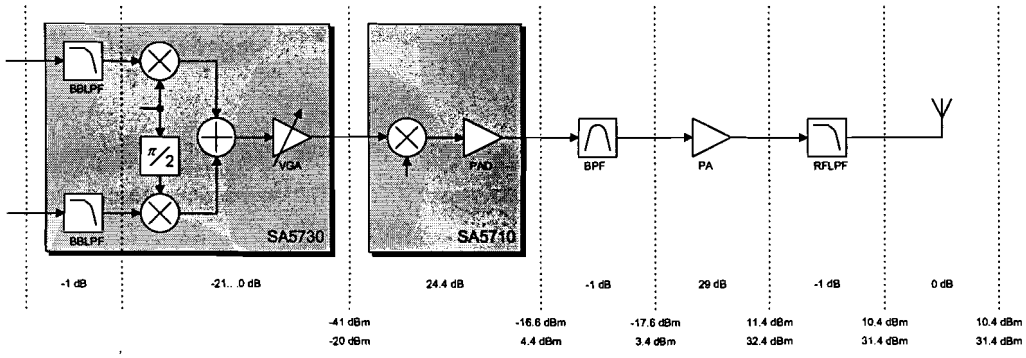

Figure 25: Power distribution of the transmitter path of the actual RF front-end.

A few things can be noted from the above figure. The output power of the SA5730 is well below its output referred IP3 [14]. The output power of the SA5710 is well below its output referred CP [19]. The input power to the PA is below its maximum input power of 7 dBm [20], however the output power in the maximum gain setting is above its output referred CP of 22.5 dBm [20]. For non-bridging applications, the maximum transmit power level is 200 mW or 23 dBm, as specified in Chapter 4. The transmit power at the antenna in the high gain setting is above this maximum transmit power level.
The output power of the PA and the transmit power at the antenna seem to indicate there is too much gain in the transmitter path. However, the excess gain is used to compensate for varying gains of the various building blocks, especially for the PAD and PA. Also the attenuation of the BPF and RFLPF filters are not specified and can easily be higher than 1 dB. Hence the given power distribution appears to be plausible.

6.2 Receiver Path

The current implementation of the receiver path of the RF front-end is very similar to the transmitter path. It uses one IF to convert the RF signal, received by the antenna, to the in-phase and quadrature signals at baseband. The first stage, which converts the signal from RF to IF, is part of the SA5710 IC. The second stage, which converts the signal from the IF to baseband, is part of the SA5730 IC. Figure 26 shows the basic building blocks of the receiver path of the actual RF front-end.

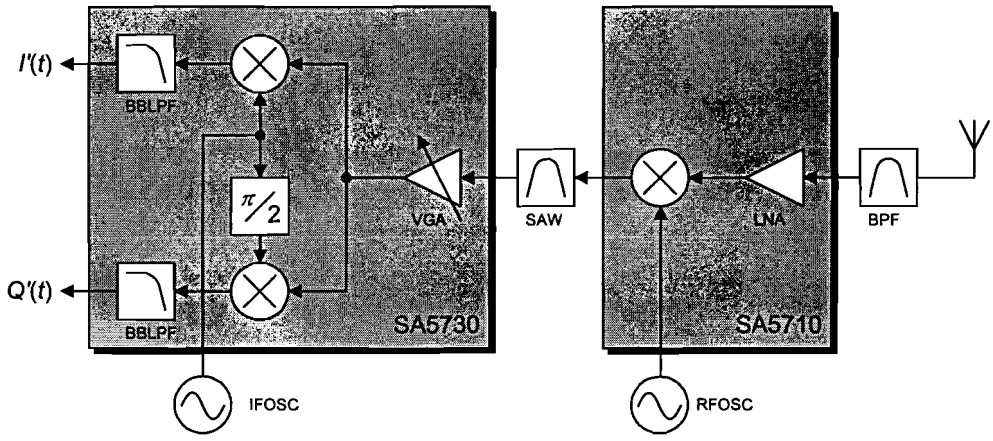

Figure 26: Receiver path of the actual RF front-end.

The following paragraphs describe the various building blocks of the receiver path in more detail.

6.2.1 Antenna

The antenna of the actual RF front-end receives the signal. As no specifications of the antenna are available, the simulation model of the antenna consists of an amplifier with a typical gain of 0 dB.

6.2.2 Band-pass Filter

The band-pass filter of the actual RF front-end passes all frequencies inside the 5 GHz ISM band with low distortion. This means the filter should be spectrally flat

and should have a linear phase in the passband. The fall-off should be high to reduce the power of out-of-band spectral components in order to reduce the power applied to the Low Noise Amplifier (LNA). As these are conflicting requirements for a filter, a trade-off should be made between the passband and stopband properties.
As only limited specifications of the band-pass filter are available, the simulation model of the band-pass filter consists of an attenuator with an attenuation of 1 dB.

6.2.3 Low Noise Amplifier

The LNA of the actual RF front-end amplifies the received signal. As the received signal generally has a low SNR, the amplifier should not introduce much internal noise as this would degrade the signal even further.
The *internal noise* of a device is often specified by the noise figure F, which is defined as the ratio of the input SNR to the output SNR, when the device is at room temperature:

$$F = \frac{SNR_i}{SNR_o} \tag{23}$$

If N noisy devices are in cascade with power gain G_{Pk} and noise figure F_k, the overall noise figure is given by Friss' formula:

$$F = F_1 + \frac{F_2 - 1}{G_{P1}} + \frac{F_3 - 1}{G_{P1}G_{P2}} + \cdots + \frac{F_N - 1}{G_{P1}G_{P2}\cdots G_{PN}} \tag{24}$$

This equation shows that when the gain of the first stage is high, the overall noise figure will be determined mainly by the noise figure of the first stage. As the LNA is the first stage of the receiver, it should have a high gain and a low noise figure. This will lead to a low overall noise figure for the receiver and will reduce the requirements for the other building blocks of the receiver, as their noise figures have little influence on the overall noise figure [21].
An important noise source in communications systems is thermal noise, which is generated by the random movement of charged particles. According to [21], it has been shown that thermal noise is additive and Gaussian distributed with zero mean. It has also been shown that the power spectral density of thermal noise is flat over a wide frequency range. Hence thermal noise can be modelled as Additive White Gaussian Noise (AWGN). The power spectral density of thermal noise is given by

$$S(f) = \frac{kT}{2} \tag{25}$$

In this equation, k is Boltzmann's constant or $1.38 \cdot 10^{-23}$ J/K and T is the temperature in Kelvin.
The amplifier amplifies not only the input signal but also the input noise. If the input noise is considered to be white and represented by its equivalent noise temperature T_i, the output noise power is given by

$$N_o = G_P \frac{kT_i}{2} 2B_N = G_P kT_i B_N \tag{26}$$

In this equation, G_P is the amplifier power gain and B_N is the noise equivalent bandwidth.
As mentioned before, the amplifier also introduces internal noise. If the internal noise power is equal to N_a than the output noise power is given by

$$\begin{aligned} N_o &= G_P kT_i B_N + N_a \\ &= G_P kB_N \left\{ T_i + \frac{N_a}{G_P kB_N} \right\} \\ &= G_P kB_N \{T_i + T_e\} \end{aligned} \tag{27}$$

In this equation, T_e is the effective noise temperature, which is related to the noise figure F and the room temperature T_0 of 290 K by [21]

$$F = 1 + \frac{T_e}{T_0} \tag{28}$$

Hence the internal noise can be modelled as AWGN with a variance σ_n^2 equal to the internal noise power, which is given by

$$N_a = G_P kB_N (F-1) T_0 \tag{29}$$

If Gaussian noise is band-limited, the noise signal $n(t)$ can be expressed in quadrature form as

$$n(t) = n_I(t)\cos(\omega t) - n_Q(t)\sin(\omega t) \tag{30}$$

The in-phase and quadrature Gaussian noise signals $n_I(t)$ and $n_Q(t)$ are uncorrelated and their variances σ_I^2 and σ_Q^2 are equal to the variance σ_n^2 of $n(t)$ [16], [21].
The simulation model of the LNA is equal to the simulation model of the VGA. Gaussian noise is added to the in-phase and quadrature components of the output signal. Two uncorrelated noise sources are used, each with a noise power or variance given by equation (29). The simulation model parameters are based on the specifications [19], which are not reprinted here because of confidentiality.

6.2.4 Mixer

The mixer at the receiver path is similar to the mixer at the transmitter path. It multiplies the received signal with the oscillator signal. The oscillator is set to a variable frequency ω_n. The spectrum of the resulting signal is equal to the spectrum of the received signal, shifted by $\pm\omega_n$, as illustrated in Figure 27. It can be seen that the wanted channel of the 5 GHz ISM band is converted from its RF frequency ω_{RF} to the IF frequency ω_{IF}.

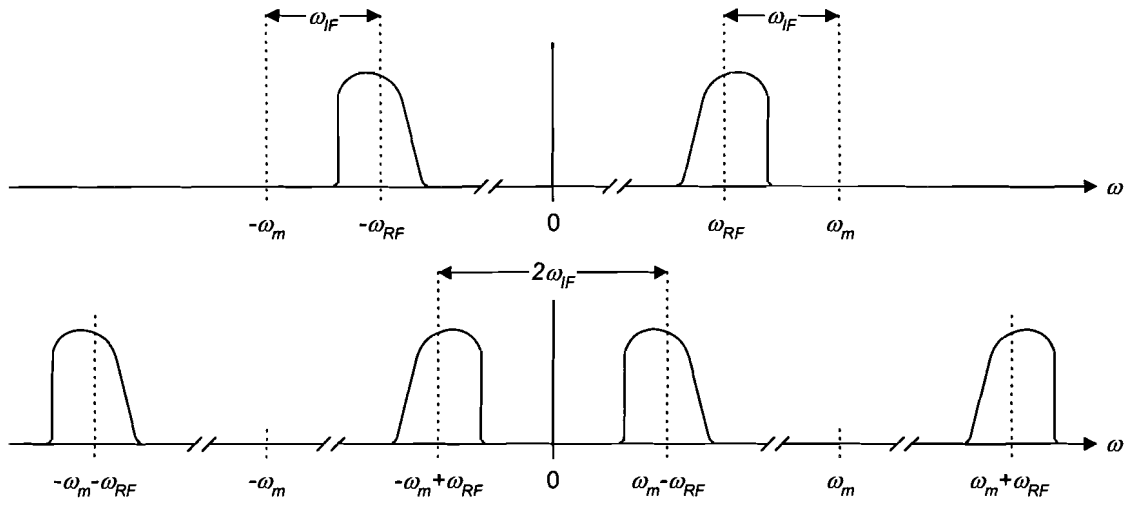

Figure 27: Simplified spectrum of received signal before and after mixing.

The simulation model of the mixer is equal to the simulation model of the mixer of the transmitter path.

6.2.5 RF Oscillator

The RF oscillator of the receiver path is the same oscillator as the RF oscillator of the transmitter path. Hence the same specifications and simulation model parameters apply.

6.2.6 Surface Acoustic Wave Filter

The Surface Acoustic Wave (SAW) filter performs the actual frequency selection, as it passes only the wanted channel, which is shifted to the IF by the mixer. It filters out all other channels, which might still be present in the input signal to the SAW filter, as they are not filtered out by the band-pass filter, which passes the entire 5 GHz ISM band.

Surface acoustic waves are waves that propagate at the surface of solids. SAW filters use the piezo-electric effect to convert electrical energy to acoustic wave energy and vice versa. As the surface acoustic waves propagate from the input to the output, the properties of the waves, such as amplitude and phase, are altered. SAW filters can have good frequency selectivity and low distortion and are especially suited for high-speed applications that require low losses and small components, such as mobile communications.

The SAW filter is characterised by scattering parameters. Scattering parameters or s-parameters characterise a N-port network using travelling waves instead of voltages or currents. The s-parameters relate the incident complex voltage waves a_k to the reflected complex voltage waves b_k, as illustrated in Figure 28 and given by equation (31) for a two-port network.

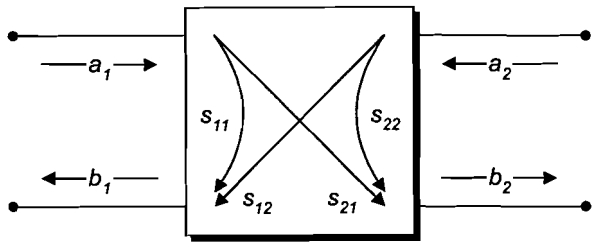

Figure 28: Scattering parameters for a two-port network.

$$\begin{aligned} b_1 &= s_{11}a_1 + s_{12}a_2 \\ b_2 &= s_{21}a_1 + s_{22}a_2 \end{aligned} \tag{31}$$

As the absolute-squared value of the variables a_k and b_k is equal to the power incident on or reflected from the two-port, the absolute-squared values of the s-parameters are related to the power transfers between the various inputs. If the device is used with a matched load and source, then the transducer power gain is given by [22]

$$G_P = |s_{21}|^2 \tag{32}$$

The simulation model of the SAW filter uses the specified amplitude and phase of s_{21} to determine the amplitude and group delay response of the actual filter. The group delay is given by

$$D(\omega) = -\frac{d}{d\omega}\arg(s_{21}(\omega)) \tag{33}$$

As the complex envelope is used to represent passband signals, the frequency response of the SAW filter is shifted to baseband. An arbitrary magnitude and group delay filter block is used in the simulations. The frequency response of the simulation model SAW filter can be found in Appendix B.

6.2.7 Variable Gain Amplifier

The VGA of the actual RF front-end amplifies the mixed signal. The gain can be set to a specific level, which is used to match the signal amplitude to the input range of the ADCs, which are located in the receiver path of the baseband module.
The simulation model of the VGA is equal to the simulation model of the LNA. The simulation model parameters are based on the specifications [14], which are not reprinted here because of confidentiality.

6.2.8 Quadrature Demodulator

The quadrature demodulator of the actual RF front-end demodulates the quadrature modulated input signal into the in-phase and quadrature components. The in-phase component is retrieved by multiplying the input signal with the oscillator signal and the quadrature component is retrieved by multiplying the input signal with the $\pi/2$ phase-shifted oscillator signal. The oscillator is set to the fixed frequency ω_{IF}. The input to the quadrature demodulator is given by

$$r(t) = I(t)\cos(\omega_{IF}t) - Q(t)\sin(\omega_{IF}t) \tag{34}$$

And the output signals are given by

$$\begin{aligned} r(t)\cos(\omega_{IF}t) &= \frac{1}{2}I(t) + \frac{1}{2}I(t)\cos(2\omega_{IF}t) - \frac{1}{2}Q(t)\sin(2\omega_{IF}t) \\ -r(t)\sin(\omega_{IF}t) &= \frac{1}{2}Q(t) - \frac{1}{2}I(t)\sin(2\omega_{IF}t) - \frac{1}{2}Q(t)\cos(2\omega_{IF}t) \end{aligned} \tag{35}$$

Equation (35) shows that the output signals contain the in-phase and quadrature components $I(t)$ and $Q(t)$ of the input signal. The output signals also contain spectral components at twice the oscillator frequency. These components are filtered out, which results in the complex baseband signal $^1/_2I(t) + j^1/_2Q(t)$. The complex baseband signal is equal to the complex envelope of the passband signal $r(t)$, except for the factor $^1/_2$, which would mean that the quadrature demodulator does not need to be included in the simulation model. However, practical quadrature demodulators suffers from non-idealities, including gain and phase imbalance, phase noise and frequency error.

Phase noise and *frequency error* can be modelled in the same way as in the case of the quadrature modulator but *phase* and *gain imbalance* cannot. The quadrature demodulator output signals in the case of gain and phase imbalance are given by

$$\begin{aligned} r(t)\cos(\omega_{IF}t) &= \frac{1}{2}I(t) + \frac{1}{2}I(t)\cos(2\omega_{IF}t) - \frac{1}{2}Q(t)\sin(2\omega_{IF}t) \\ -g_e r(t)\sin(\omega_{IF}t + \varphi_e) &= \frac{1}{2}g_e Q(t)\cos(\varphi_e) + \frac{1}{2}g_e I(t)\sin(\varphi_e) \\ &\quad -\frac{1}{2}g_e I(t)\sin(2\omega_{IF}t + \varphi_e) - \frac{1}{2}g_e Q(t)\cos(2\omega_{IF}t + \varphi_e) \end{aligned} \tag{36}$$

In this equation, the in-phase signal is chosen as the reference signal and g_e and φ_e are the gain and phase of the quadrature signal relative to the in-phase signal. Just like practical quadrature modulators, practical quadrature demodulators introduce non-linear distortion and conversion gain or loss. As the specifications of the SA5730 [14] only specify the gain and the non-linear behaviour of the entire IC, the gain and non-linearity of the quadrature demodulator itself are not known. The simulation model uses a linear model with unit gain for the quadrature demodulator and uses a non-linear model for the amplifier of the SA5730 to account for the gain and the non-linearities of the entire IC.

The simulation model of the quadrature demodulator uses equations (11), (12) and (36) to generate the in-phase and quadrature signals at baseband, including gain and phase imbalance, phase noise and frequency error. The components at twice the oscillator frequency are not generated by the simulation model. The simulation model of the quadrature demodulator can be found in Appendix A.

6.2.9 IF Oscillator

The IF oscillator of the receiver path is the same oscillator as the IF oscillator of the transmitter path. Hence the same specifications and simulation model parameters apply.

6.2.10 Baseband Low-pass Filters

The baseband low-pass filters of the actual RF front-end act as anti-aliasing filters for the ADC that follow the RF front-end. For the simulation model, a filter has been designed using FDS, which matches the actual baseband low-pass filters [14] as good as possible. The simulation model filter is a fourth order, Elliptic low-pass filter. The frequency response of the simulation model filter can be found in Appendix B.
As with the baseband low-pass filters of the transmitter path, the simulation model of the baseband low-pass filters of the receiver path uses a single filter block to filter the complex baseband signal.

6.2.11 Power Distribution

According to Chapter 4, the receiver should operate correctly for received power levels ranging from –82 dBm to –30 dBm. This is used as the reference for the power distribution calculation, as shown in Figure 29.

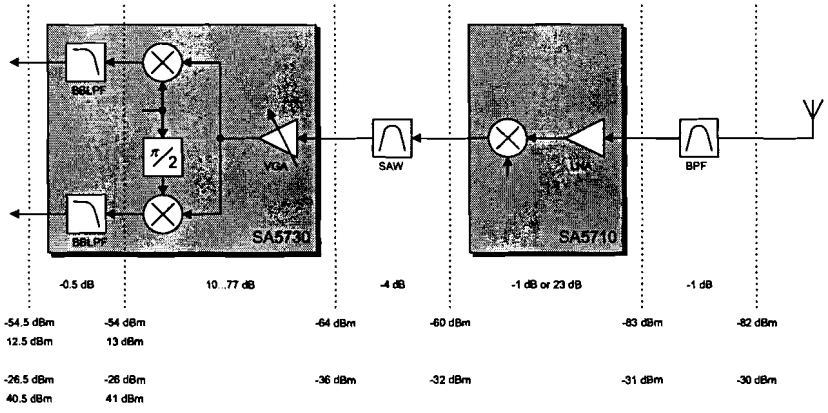

Figure 29: Power distribution of the receiver path of the actual RF front-end.

A few things can be noted from the above figure. The SA5710 has a gain of 23 dB for low received power levels and a gain of –1 dB for high received power levels. The output power of the SA5710 is well below its output referred CP [19]. The input power to the SA5730 is well below its input referred IP3 [14].
The output power of the SA5730 should be matched to the input range of the ADCs, which directly follow the IC. According to the specifications of the SA5730 [14], the input range of the ADCs is 1 V_{pp}, which is 1 / $2\sqrt{2}$ or 0.35 V_{rms}. In a 50 Ω system, this is equal to a maximum input power of $10\log(0.35^2 \times 1000 / 50)$ or 4.0 dBm. According to Chapter 3, the PAP ratio of an OFDM signal is upper limited by the number of subcarriers, which is 52. Using this maximum PAP ratio of 10log52 or 17 dB, the average input power to the ADCs should be 4.0 – 17 or –13 dBm. The power distribution shows that both the minimum and maximum receiver power levels can be converted to this power level. Hence the given power distribution appears plausible.

7
Simulations

In the previous two chapters, simulation models have been derived for the baseband module and the RF front-end of the IEEE 802.11a compliant modem. The simulation models of the complete transmitter and receiver path, which can be found in Appendix A, are created using these simulation models and are based on the available specifications. This chapter discusses the simulations that were performed using these simulation models and interprets the results.

7.1 Transmitter Path

As mentioned before, the simulation model of the complete transmitter path can be found in Appendix A. The simulation model uses 64-QAM modulation symbols. This modulation method is the most demanding case for the IEEE 802.11a standard as the constellation is dense. The simulation model uses an additional gain block after the baseband module transmitter block (BBTX) to set the correct output power of the baseband module. The simulation model implements no gain imbalance, phase imbalance or frequency offset. All other block parameters are set as specified in Chapter 6. To determine the effect of the transmitter path on the OFDM signal and to determine the spectrum of the transmitted signal, two simulations are done.

7.1.1 Minimum VGA Gain

For the first simulation of the transmitter path the gain of the VGA is set to the minimum level of –21 dB. This results in low signal power levels and assures that all amplifiers are operated well below the CP. This causes a minimal amount of intermodulation interference.
Figure 30 shows spectra of the simulated OFDM signal at various points of the transmitter path. A few things can be noted from the figure. After the BBLPF filters the side lobes have been reduced. After the PA the signal has been amplified and side lobes have been introduced. The side lobes occur because of intermodulation, mainly at the PA.
Figure 31 shows the spectrum of the simulated OFDM signal at the antenna. The top plot shows the spectral mask of the IEEE 802.11a standard. It can be seen that the spectrum is well below the spectral mask. The bottom plot shows the limits of the spectral flatness requirements of the IEEE 802.11a standard. It can be seen that the spectrum is within the limits.
Figure 32 shows constellation diagrams of the edge and middle subcarriers of the simulated OFDM signal at various points of the transmitter path. A few thing can be noted from the figure. After the BBLPF filters the edge subcarrier has experienced a phase offset compared to the middle subcarrier. This is because the group delay of the BBLPF filters is different for both subcarriers, as can be seen in Appendix B. After the PA the signal has been amplified and noise has been added. The additional noise is caused by intermodulation.

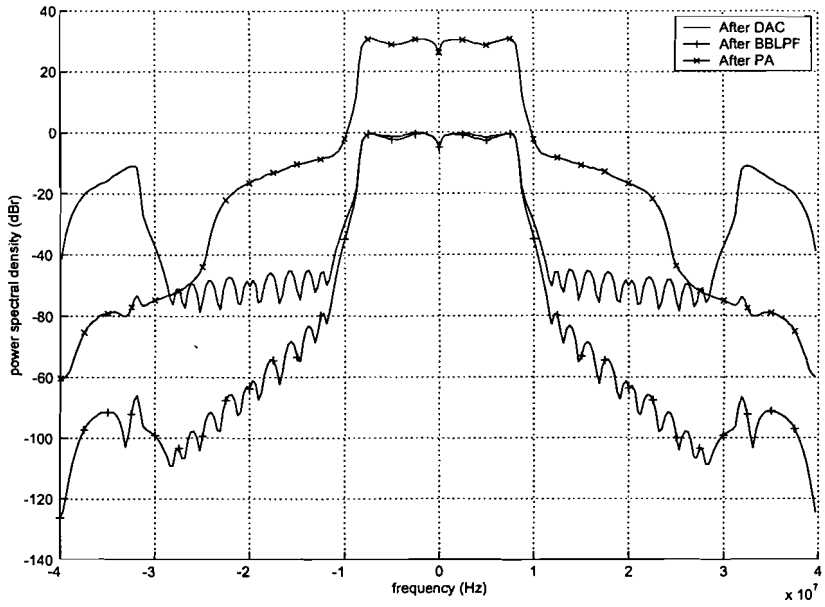

Figure 30: Spectra of the simulated OFDM signal at various points of the transmitter path.

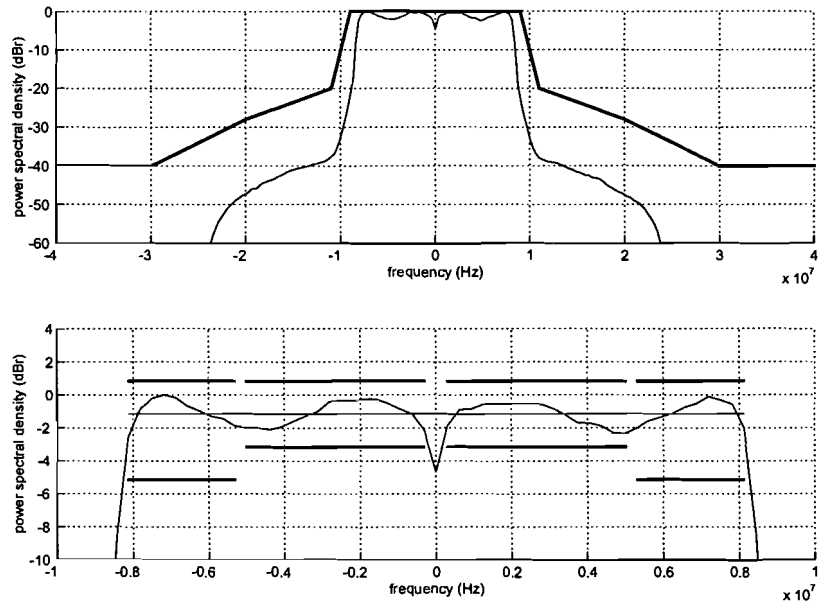

Figure 31: Spectrum of the simulated OFDM signal at the antenna. The bold lines represent the spectral mask (top plot) and the spectral flatness requirements (bottom plot).

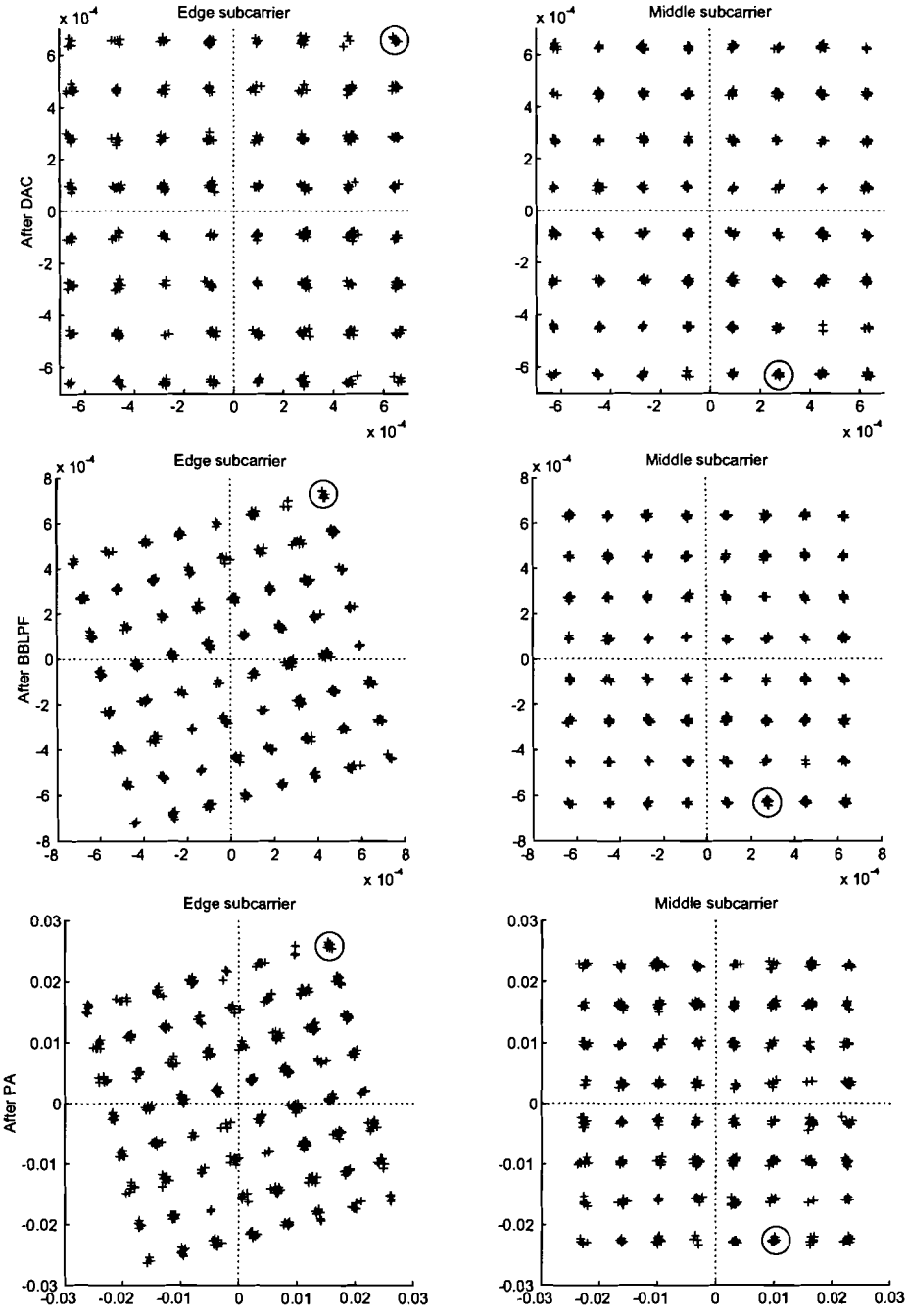

Figure 32: Constellation diagrams of the edge and middle subcarriers of the simulated OFDM signal at various points of the transmitter path.

7.1.2 Power Amplifier used at the Compression Point

For the second simulation of the transmitter path the gain of the VGA is set to such a level that the PA is operated at the CP. This increases the amount of intermodulation interference.

Figure 33 shows the spectra of the simulated OFDM signal at various points of the transmitter path. It can be seen that the side lobes have been significantly increased after the PA. This shows that intermodulation interference is mainly caused by the PA.

Figure 34 shows the spectrum of the simulated OFDM signal at the antenna. The top plot shows the spectral mask of the IEEE 802.11a standard. It can be seen that the spectrum is no longer below the spectral mask. The bottom plot shows the limits of the spectral flatness requirements of the IEEE 802.11a standard. It can be seen that the spectrum is still within the limits. If the simulation results are compared to the results of the previous simulation, it can be seen that the shape of the spectrum of the main lobe is similar. The increased amount of intermodulation has no visible effect on the shape of the spectrum of the main lobe, which is mainly determined by the frequency response of the filters.
Figure 35 shows constellation diagrams of the edge and middle subcarrier of the simulated OFDM signal at various points of the transmitter. It can be seen that noise has been added after the PA because of intermodulation.

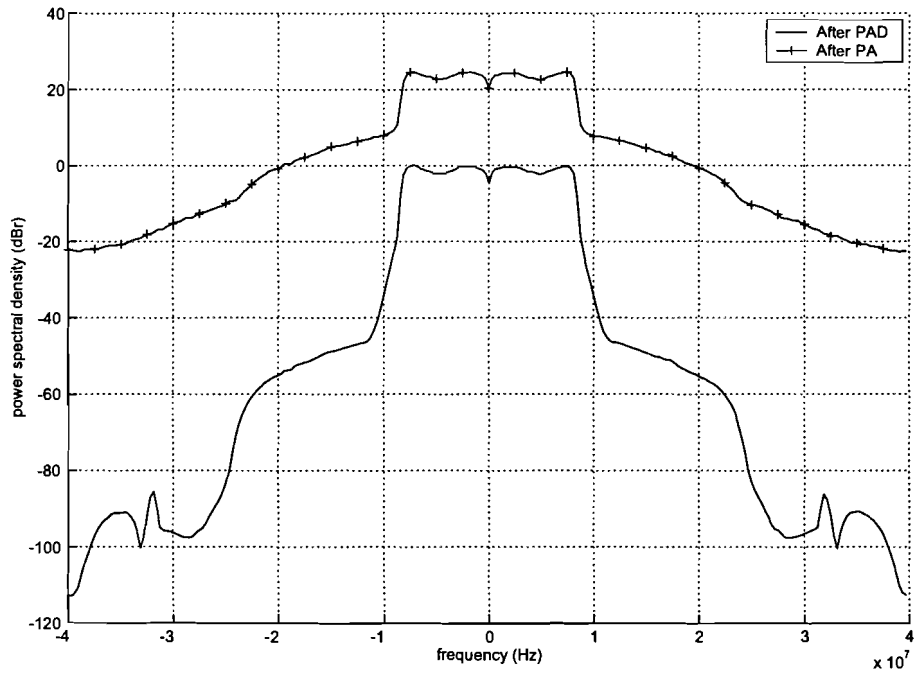

Figure 33: Spectra of the simulated OFDM signal at various points of the transmitter path.

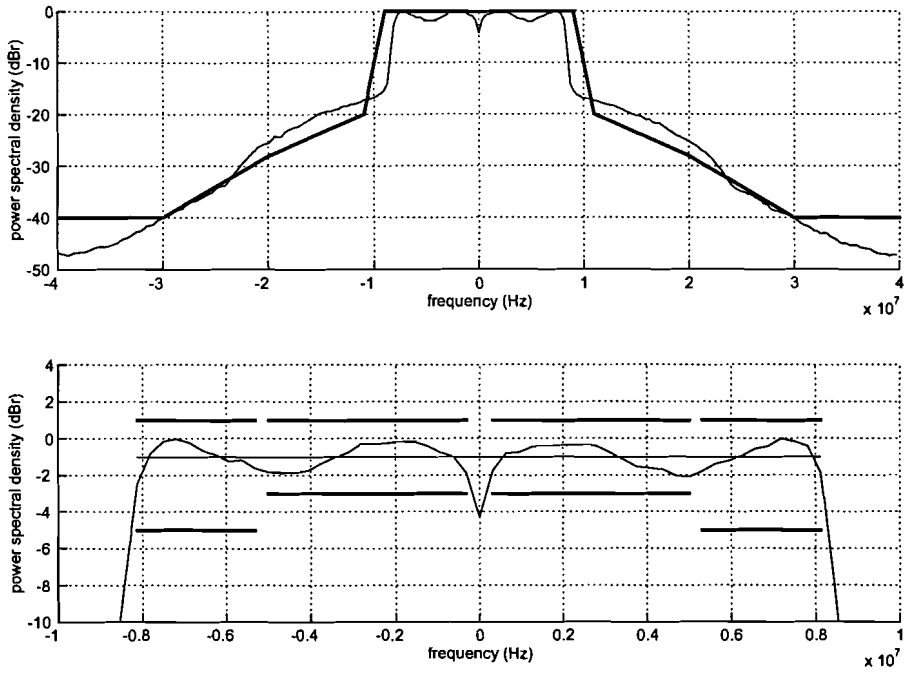

Figure 34: Spectrum of the simulated OFDM signal at the antenna. The bold lines represent the spectral mask (top plot) and the spectral flatness requirements (bottom plot).

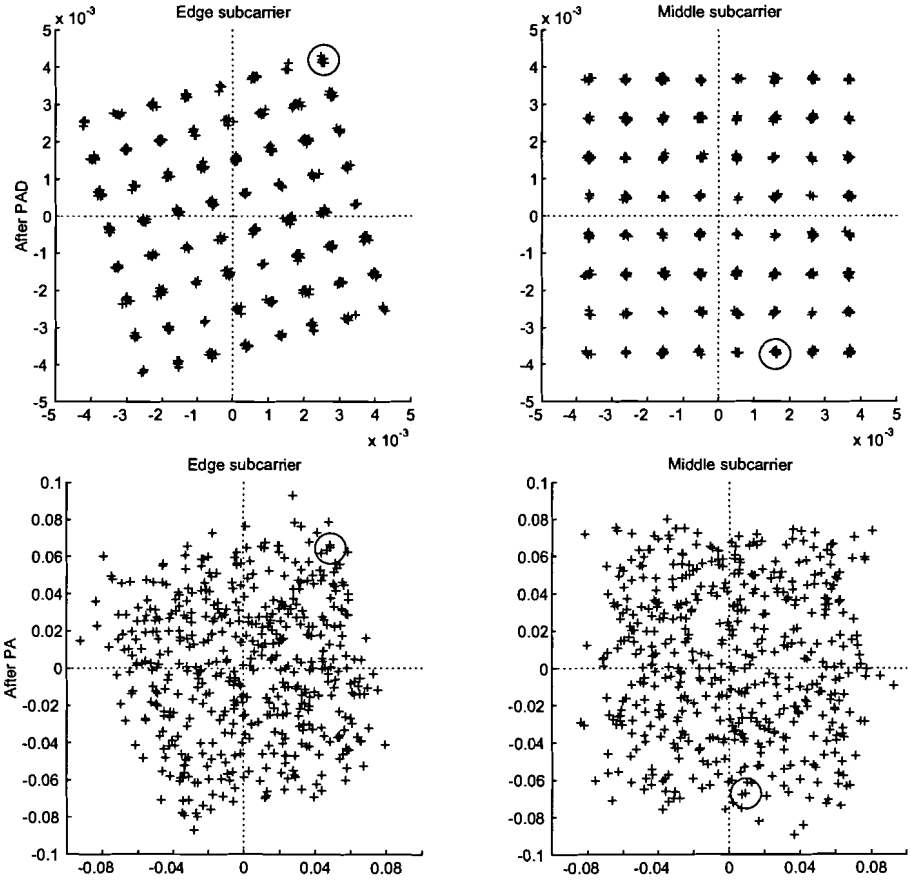

Figure 35: Constellation diagrams of the edge and middle subcarriers of the simulated OFDM signal at various points of the transmitter path.

7.1.3 Conclusions

For minimum VGA gain, the spectrum of the transmitted OFDM signal satisfies the spectral requirements of the IEEE 802.11a standard. If the VGA gain is set to such a level that the PA is operated at the CP, the spectrum of the transmitted OFDM signal no longer satisfies this requirement. In this case the transmit power is 21.5 dBm, which is below the maximum allowed transmit power for non-bridging applications of 200 mW or 23 dBm as specified in Chapter 4. This means that the current design of the transmitter path cannot achieve the maximum allowed transmit power. If the transmitter is required to achieve the maximum transmit power, another PA with a higher CP must be used.

7.2 Receiver Path

As mentioned before, the simulation model of the complete receiver path can be found in Appendix A. The simulation model reads the transmitted OFDM signal generated by the transmitter path simulation model and uses an additional gain block to set the correct received power. The simulation model implements no gain imbalance, phase imbalance or frequency offset. All other block parameters are set as specified in Chapter 6. To determine the effect of the receiver path on the OFDM signal, two simulations are done.

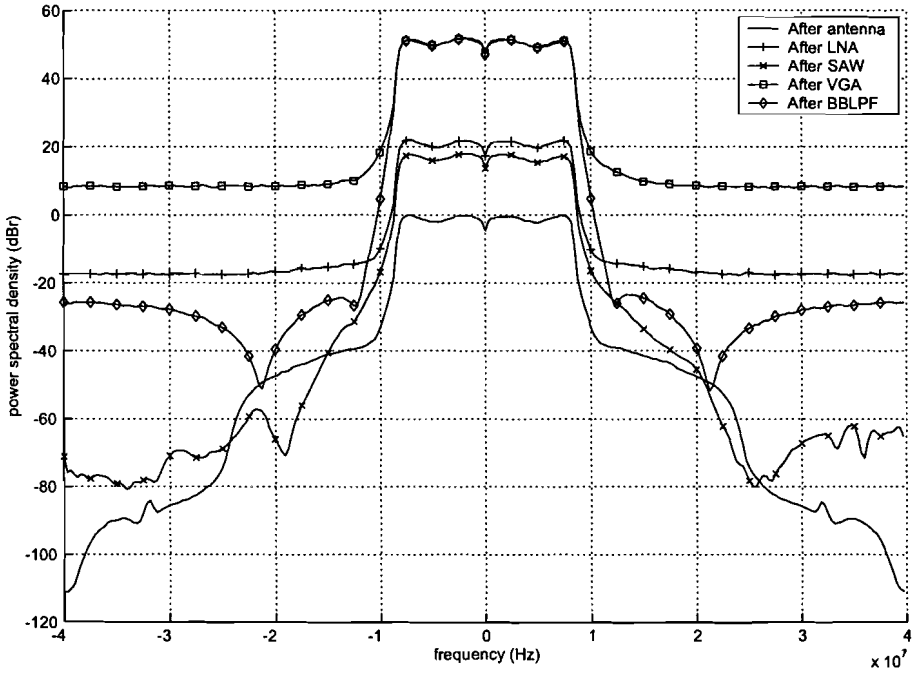

Figure 36: Spectra of the simulated OFDM signal at various points of the receiver path.

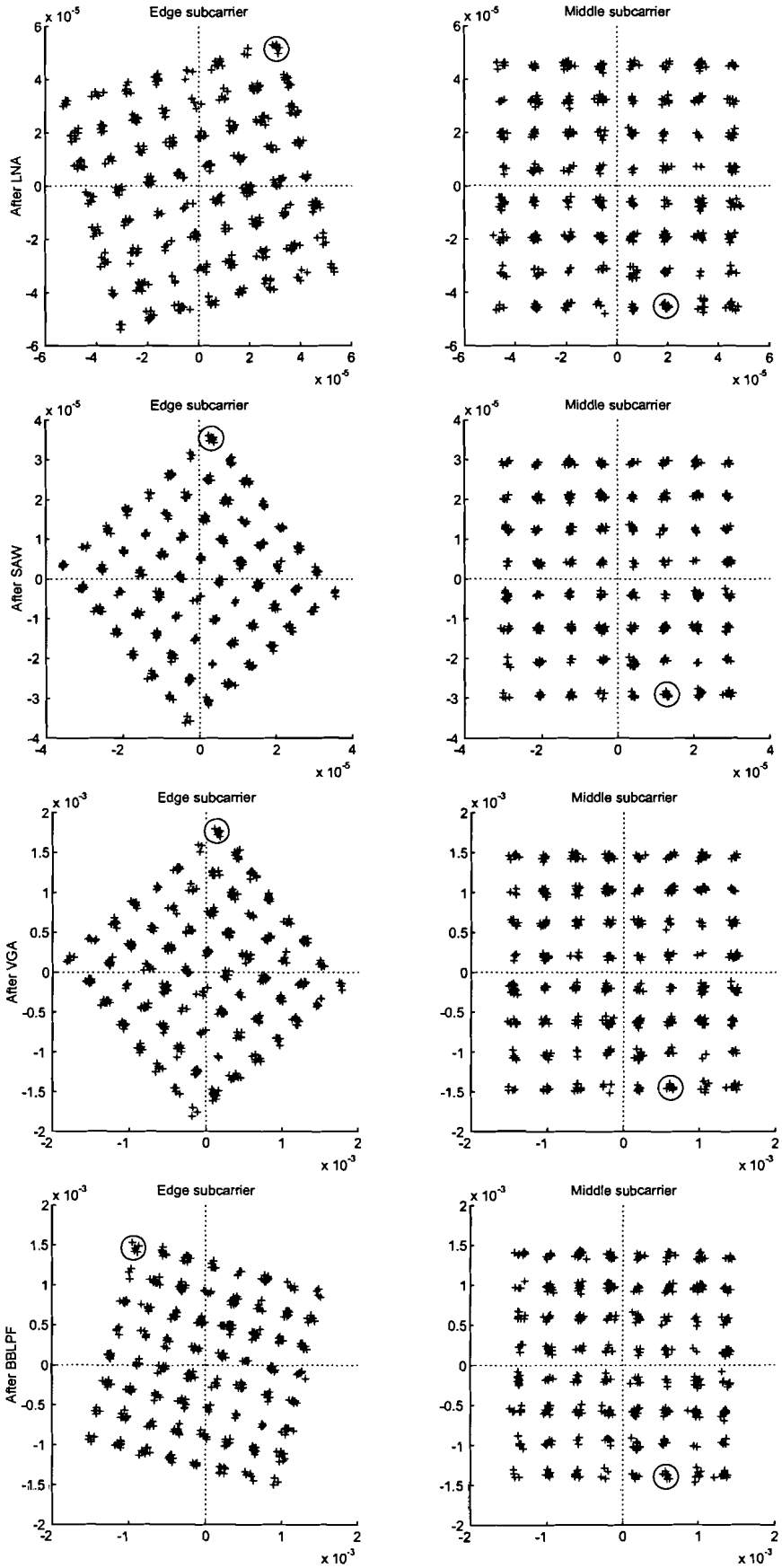

Figure 37: Constellation diagrams of the edge and middle subcarrier of the simulated OFDM symbol at various points of the receiver path.

7.2.1 Minimum Received Power

For the first simulation of the receiver path, the transmitted OFDM signal generated by the transmitter path simulation model with the gain of the VGA set to the minimum level is used as the received signal. The power of the received signal is set to the minimum received power specified by the IEEE 802.11a standard [12], which is –65 dBm for 64-QAM. This results in low signal power levels. This causes a minimal amount of intermodulation interference as all amplifiers are operated well below the CP but increases the impact of internal noise of the amplifiers.

Figure 36 shows spectra of the simulated OFDM signal at various points of the receiver path. A few thing can be noted from the figure. After the LNA and VGA the signal has been amplified and a noise floor has been added because of the internal noise. After the SAW and BBLPF filters the out-of-band emissions have been reduced.

Figure 37 shows constellation diagrams of the edge and middle subcarriers of the simulated OFDM signal at various points of the receiver path. A few things can be noted from the figure. After the LNA and VGA the signal has been amplified and noise has been added. The additional noise is mainly caused by the internal noise of the amplifiers. After the SAW and BBLPF filters the edge subcarrier has experienced a phase offset compared to the middle subcarrier. This is because the group delay of the filters is different for both subcarriers, as can be seen in Appendix B. After the BBLPF filters distinct groups of modulation symbols are present, which indicates that the baseband module might be able to recover the transmitted binary data without error.

7.2.2 Maximum Received Power

For the second simulation of the receiver path, the transmitted OFDM signal generated by the transmitter path simulation model with the gain of the VGA set to the minimum level is used as the received signal. The power of the received signal is set to the maximum received power specified by the IEEE 802.11a standard [12], which is –30 dBm for all modulation methods. This increases the amount of intermodulation interference as the LNA is operated close to the CP but reduces the impact of the internal noise of the amplifiers.

Figure 38 shows constellation diagrams of the edge and middle subcarriers of the simulated OFDM signal after the LNA. It can be seen that noise has been added, mainly because of intermodulation. Distinct groups of modulation symbols are no longer present, which indicate that the baseband module might not be able to recover the transmitted binary data.

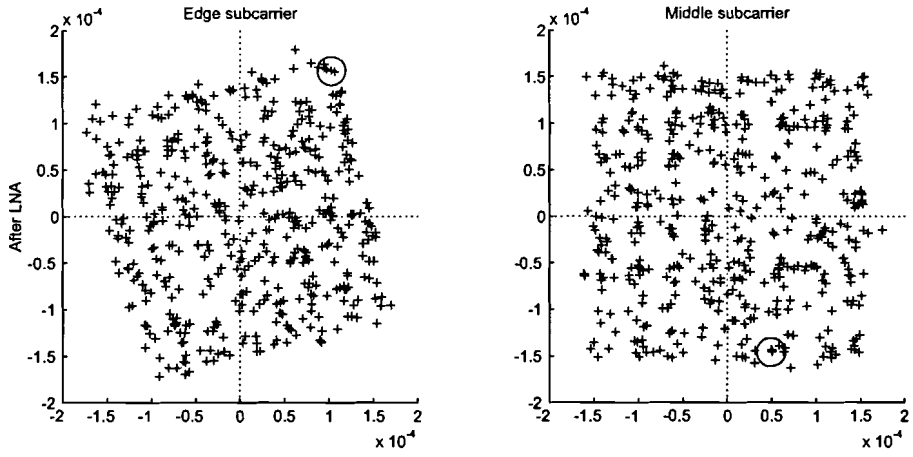

Figure 38: Constellation diagrams of the edge and middle subcarriers of the simulated OFDM signal after the LNA.

7.2.3 Conclusions

For minimum received power, the receiver adds only limited noise to the OFDM signal. For maximum received power, the receiver adds more noise to the OFDM signal because of intermodulation. This is because the LNA is operated close to the CP. Using a BPF with a higher attenuation would reduce the power to the LNA and thus reduce the amount of intermodulation interference.

8
Conclusions

The subject of this Master's thesis report was the design of a simulation model of the RF front-end of the IEEE 802.11a compliant modem. The principles of OFDM, the IEEE 802.11a standard and the current design of the actual modem have been discussed. The effects of the components of the RF front-end on the OFDM signal have been determined, especially the effects of imperfections, such as gain and phase imbalance, phase noise, frequency offset, timing offset and non-linearity. A simulation model of the RF front-end and a limited simulation model of the baseband module have been designed and some simulations have been performed. This chapter presents the conclusions derived during the Master's thesis and recommendations for further work.

8.1 Conclusions

Based on the simulation results presented in the previous chapter, the following conclusions can be made.
For low transmit powers, the spectrum of the transmitted OFDM signal satisfies the spectral requirements of the IEEE 802.11a standard. The spectrum is well below the spectral mask and is within the spectral flatness limits. For high transmit powers, if the PA is operated at the CP, the amount of intermodulation interference increases. The spectrum no longer satisfies the spectral requirements of the IEEE 802.11a standard. The spectrum is no longer below the spectral mask, however it is still within the spectral flatness limits. If the transmitter is required to achieve the maximum transmit power for non-bridging applications, another PA with a higher CP must be used.
For low received power levels, the receiver adds only limited noise to the OFDM signal, which indicates that the baseband module might be able to recover the transmitter binary data without error. For high received power levels, the amount of intermodulation interference increases. For the maximum received power, the LNA is operated close to the CP and simulations indicate that the baseband module might not be able to recover the transmitted binary data. Reducing the power to the LNA by using a BPF with a higher attenuation is a solution.

8.2 Recommendations

The simulation model of the RF front-end is based on limited specifications. If additional specifications become available the simulation model can be improved, e.g. by using a more detailed model or by modelling additional imperfections.
The simulation model of the baseband module derived in this report is a limited model as it is only meant to be a tool for simulations of the RF front-end. As mentioned in Chapter 1, a complete simulation model of the baseband module already exists. This simulation model can be used together with the simulation model of the RF front-end to perform additional simulations, such as

- Simulations to compare the performance for the various modulation types.
- Simulations to determine the effect of imperfections on the BER performance.
- Simulations to determine what imperfections can be tolerated for a limited BER degradation, e.g. what amount of intermodulation interference caused by the PA or LNA can be tolerated.
- Simulations to determine the effect of ADC.

Measurements of the actual RF front-end should be compared to simulation results to determine the validity of the simulation model.

Appendix A
Simulation Models

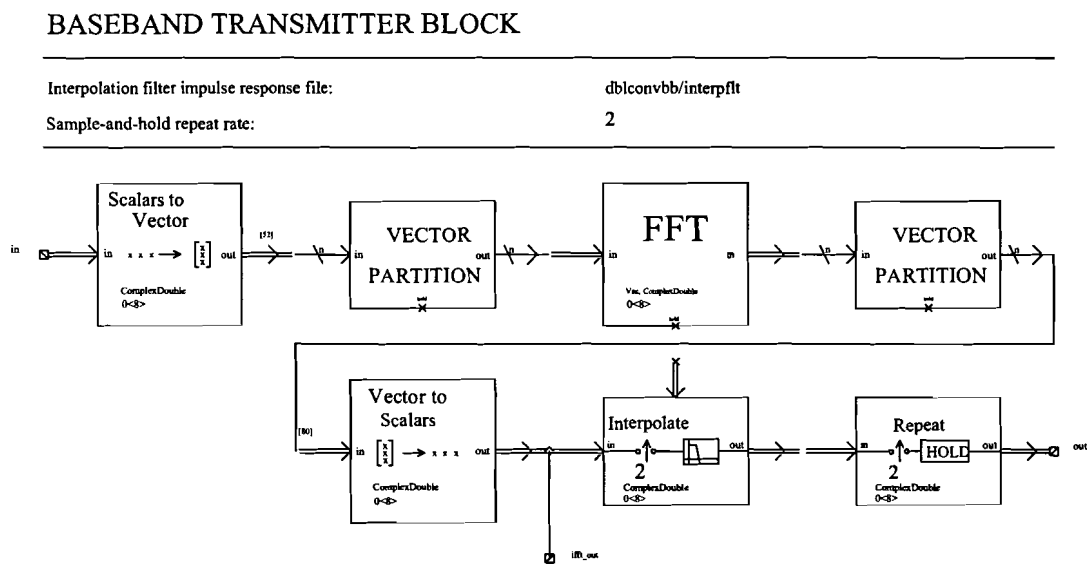

Figure 39: Simulation model of the baseband module transmitter path.

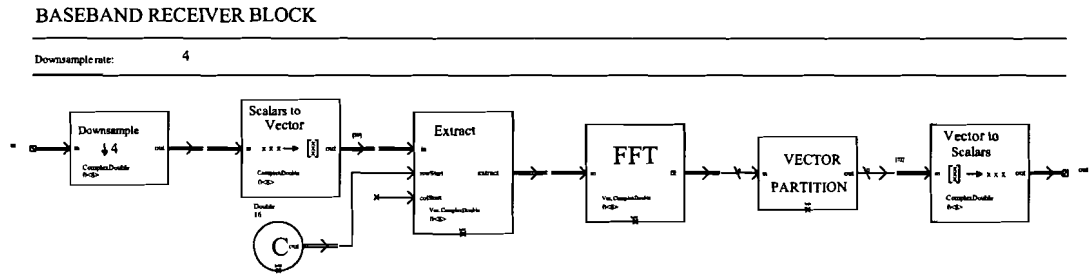

Figure 40: Simulation model of the baseband module receiver path.

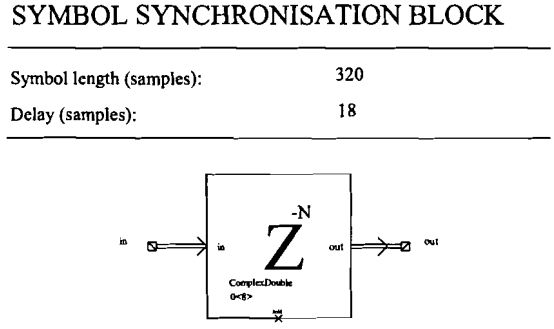

Figure 41: Simulation model of the baseband module symbol synchronisation block.

QUADRATURE MODULATOR BLOCK

Sampling frequency (fs, Hz):	8.0e7
Gain error factor (ge):	1.0
Phase error (phie, deg):	0.0
Frequency error (fe, Hz):	0.0

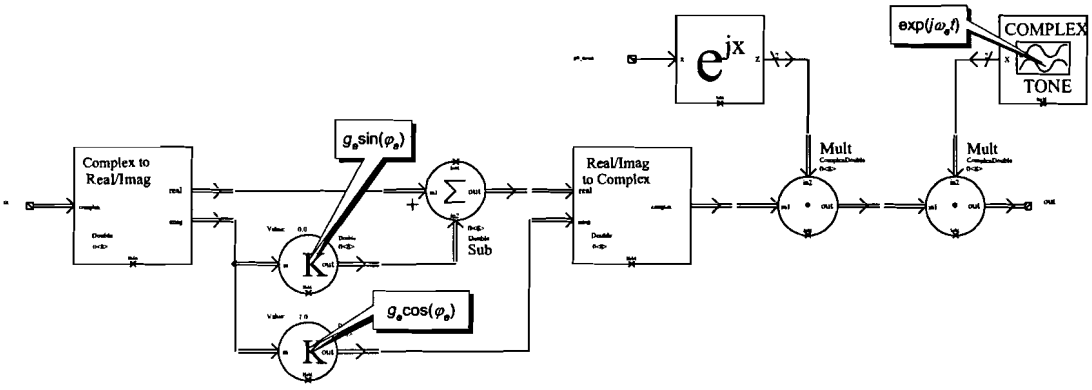

Figure 42: Simulation model of the RF front-end quadrature modulator.

OSCILLATOR BLOCK

Sampling frequency (fs, Hz):	8.0e7
Total integrated phase noise power (K, dBc):	-40.0
Phase noise (dBc/Hz):	-125.0
at frequency (Hz):	1.0e6
3-dB linewidth set to 9935.568964 Hz.	
Carrier power (C, dBm):	10.0

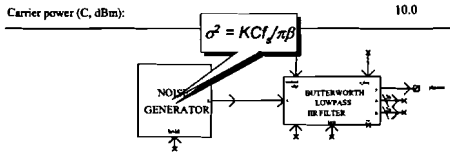

Figure 43: Simulation model of the RF front-end oscillators.

NON-LINEAR AMPLIFIER

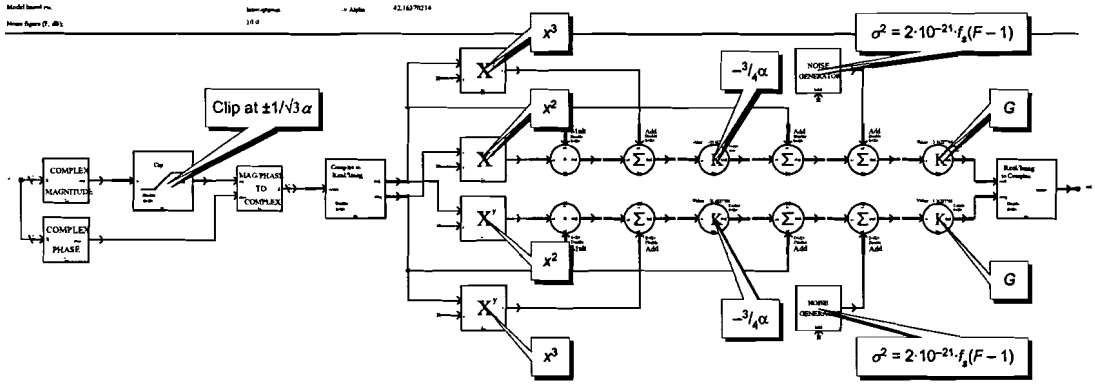

Figure 44: Simulation model of the RF front-end non-linear amplifiers.

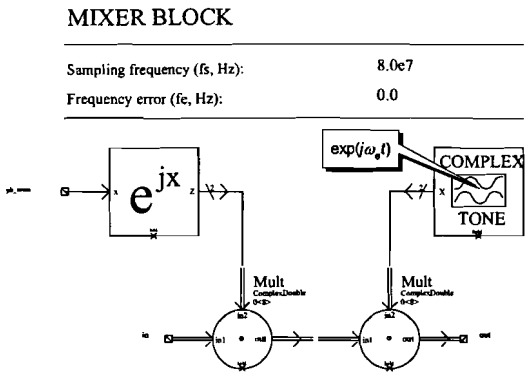

Figure 45: Simulation model of the RF front-end mixers.

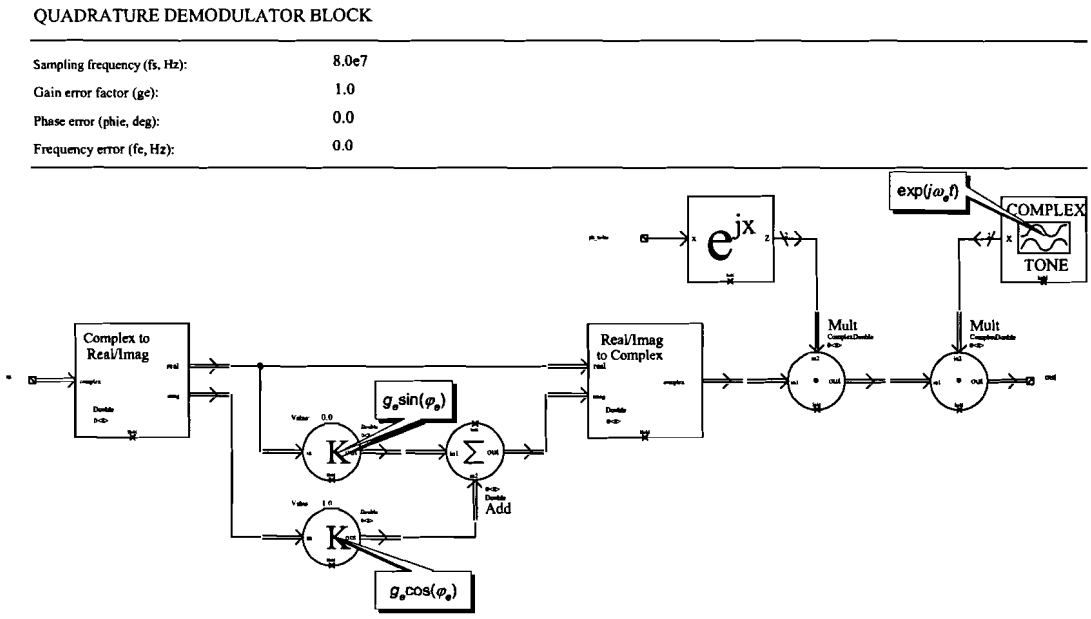

Figure 46: Simulation model of the RF front-end quadrature demodulator.

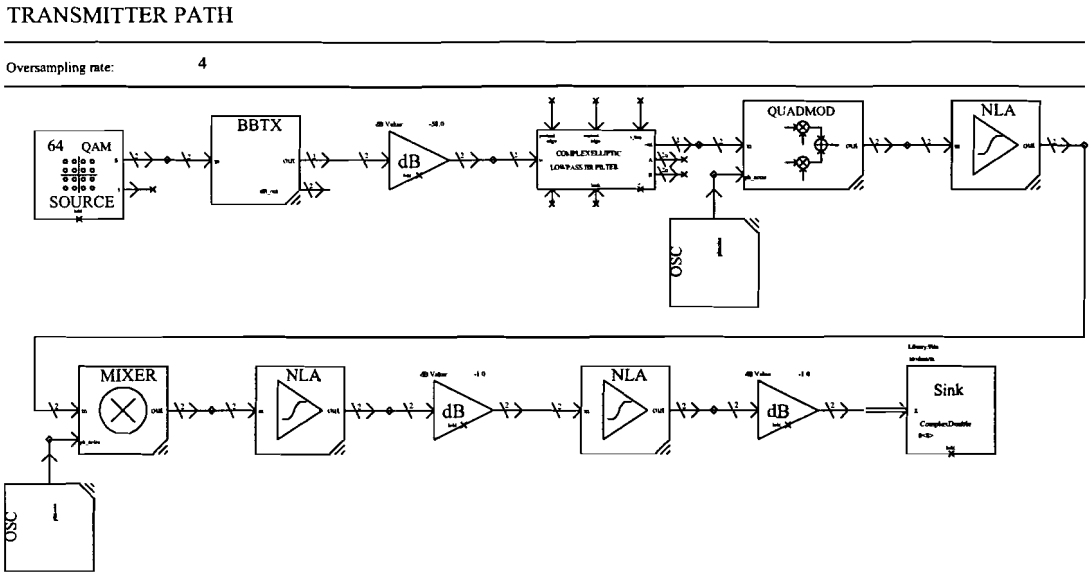

Figure 47: Simulation model of complete transmitter path.

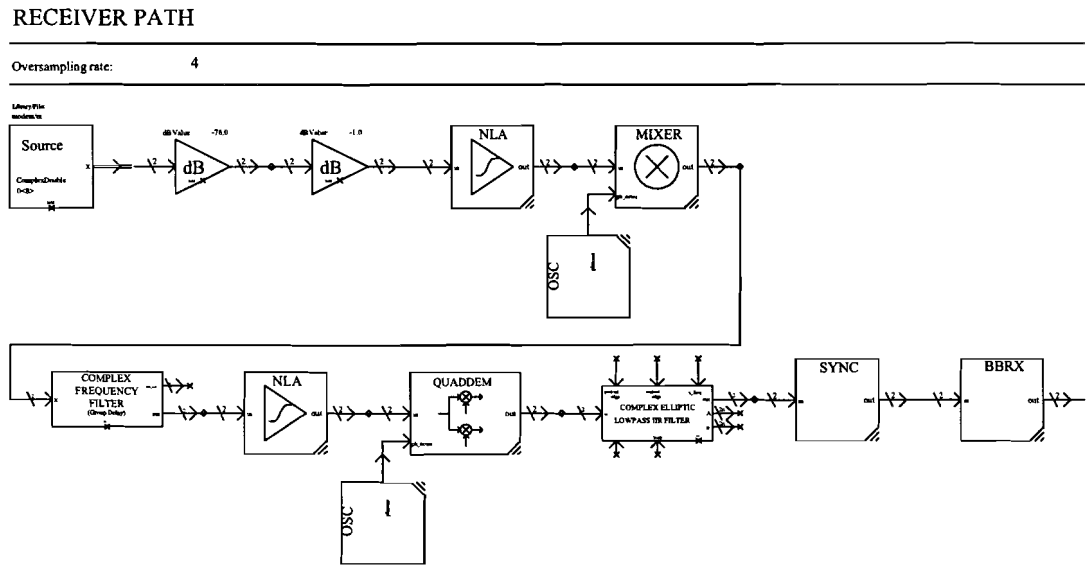

Figure 48: Simulation model of complete receiver path.

Appendix B
Filter Frequency Responses

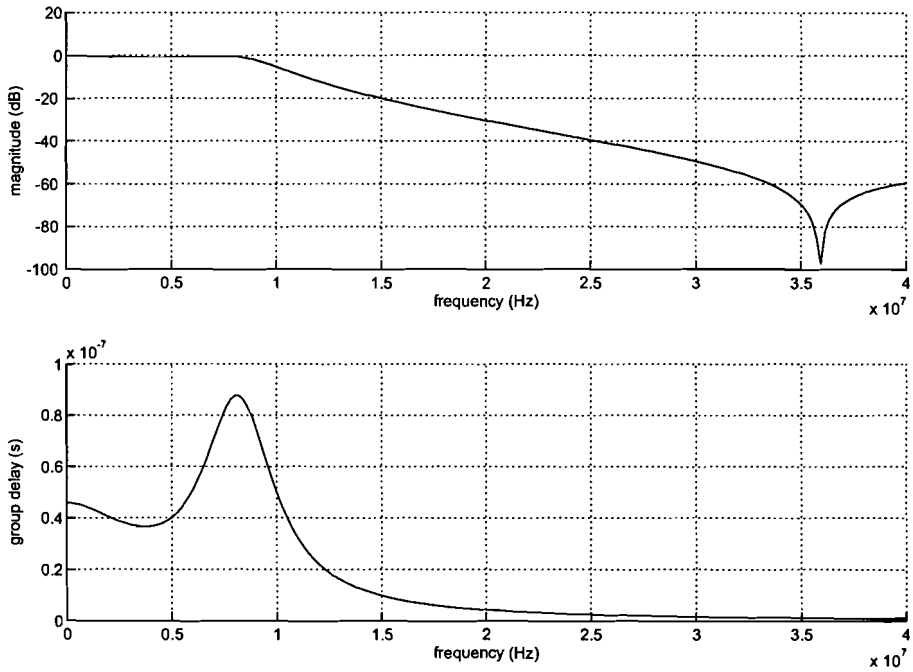

Figure 49: RF front-end transmitter baseband low-pass filter.

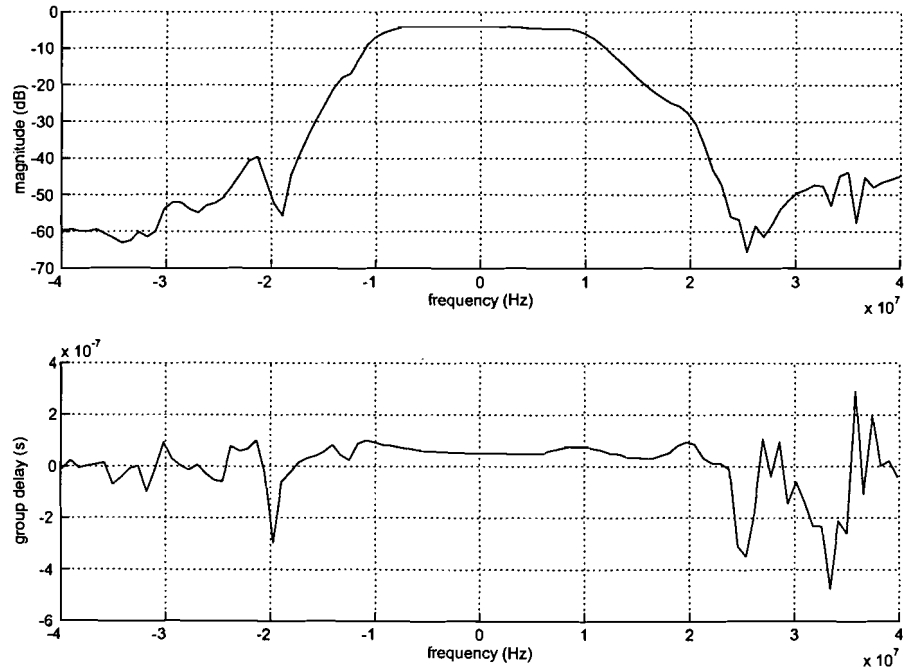

Figure 50: RF front-end receiver SAW filter.

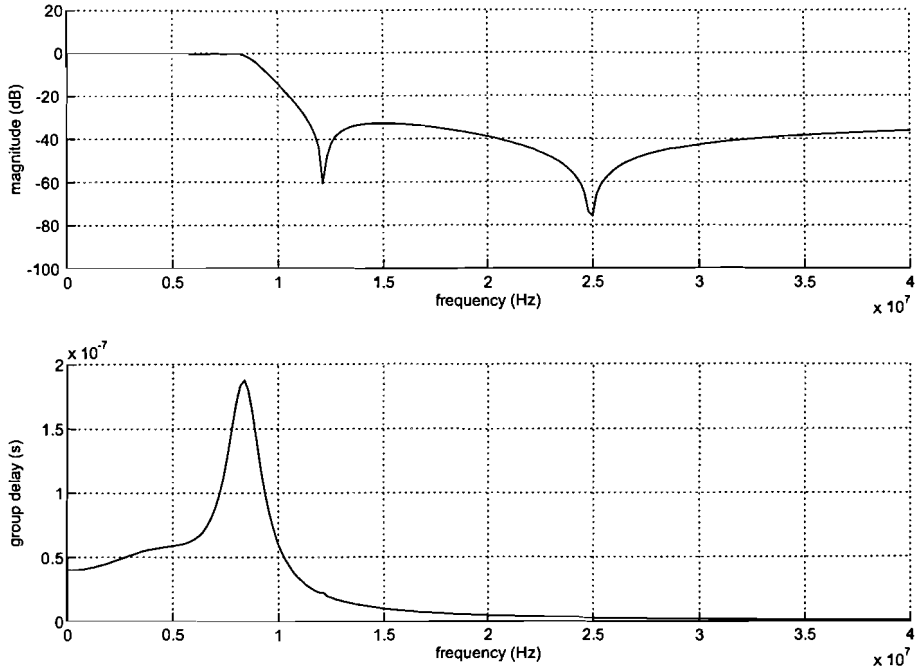

Figure 51: RF front-end receiver baseband low-pas filter.

Appendix C
Amplifier Response to a Quadrature Modulated Signal

In Chapter 6, a simulation model of a non-linear amplifier is derived. To determine the simulation model, the amplifier response to a quadrature modulated signal is used. In this appendix, the amplifier response to a quadrature modulated signal is calculated.
The amplifier model is given by

$$y(t) = G\left\{x(t) - \alpha x^3(t)\right\}$$

The quadrature modulated signal is given by

$$x(t) = I(t)\cos(\omega t) - Q(t)\sin(\omega t)$$

In the following calculations, the in-phase and quadrature components $I(t)$ and $Q(t)$ will be written without their argument for the sake of brevity.
First, the square of the input signal is calculated:

$$\begin{aligned} x^2(t) &= I^2\cos^2(\omega t) - 2IQ\cos(\omega t)\sin(\omega t) + Q^2\sin^2(\omega t) \\ &= \frac{1}{2}I^2\{1+\cos(2\omega t)\} - IQ\{\sin(2\omega t)+\sin(0)\} + \frac{1}{2}Q^2\{1-\cos(2\omega t)\} \\ &= \frac{1}{2}\{I^2+Q^2\} + \frac{1}{2}\{I^2-Q^2\}\cos(2\omega t) - IQ\sin(2\omega t) \end{aligned}$$

The third power of the input signal is calculated by multiplying the previous result by the input signal:

$$\begin{aligned} x^3(t) &= \{I\cos(\omega t) - Q\sin(\omega t)\}x^2(t) \\ &= \frac{1}{2}I\{I^2+Q^2\}\cos(\omega t) + \frac{1}{2}I\{I^2-Q^2\}\cos(2\omega t)\cos(\omega t) - I^2Q\sin(2\omega t)\cos(\omega t) \\ &\quad -\frac{1}{2}Q\{I^2+Q^2\}\sin(\omega t) - \frac{1}{2}Q\{I^2-Q^2\}\cos(2\omega t)\sin(\omega t) + IQ^2\sin(2\omega t)\sin(\omega t) \\ &= \frac{1}{2}I\{I^2+Q^2\}\cos(\omega t) + \frac{1}{4}I\{I^2-Q^2\}\{\cos(3\omega t)+\cos(\omega t)\} - \frac{1}{2}I^2Q\{\sin(3\omega t)+\sin(\omega t)\} \\ &\quad -\frac{1}{2}Q\{I^2+Q^2\}\sin(\omega t) - \frac{1}{4}Q\{I^2-Q^2\}\{\sin(3\omega t)-\sin(\omega t)\} + \frac{1}{2}IQ^2\{\cos(\omega t)-\cos(3\omega t)\} \end{aligned}$$

The last equation contains third order terms $\cos(3\omega t)$ and $\sin(3\omega t)$. However, these are out of band and can be ignored:

$$
\begin{aligned}
x^3(t) &= \frac{1}{2} I\{I^2 + Q^2\}\cos(\omega t) + \frac{1}{4} I\{I^2 - Q^2\}\cos(\omega t) - \frac{1}{2} I^2 Q \sin(\omega t) \\
&\quad - \frac{1}{2} Q\{I^2 + Q^2\}\sin(\omega t) + \frac{1}{4} Q\{I^2 - Q^2\}\sin(\omega t) + \frac{1}{2} IQ^2 \cos(\omega t) \\
&= \left\{\frac{1}{2} I^3 + \frac{1}{2} IQ^2 + \frac{1}{4} I^3 - \frac{1}{4} IQ^2 + \frac{1}{2} IQ^2\right\}\cos(\omega t) \\
&\quad - \left\{\frac{1}{2} I^2 Q + \frac{1}{2} I^2 Q + \frac{1}{2} Q^3 - \frac{1}{4} I^2 Q + \frac{1}{4} Q^3\right\}\sin(\omega t) \\
&= \left\{\frac{3}{4} I^3 + \frac{3}{4} IQ^2\right\}\cos(\omega t) - \left\{\frac{3}{4} Q^3 + \frac{3}{4} I^2 Q\right\}\sin(\omega t)
\end{aligned}
$$

Using this expression for $x^3(t)$, the amplifier response is given by

$$
\begin{aligned}
y(t) &= G\left\{I - \frac{3}{4}\alpha I^3 - \frac{3}{4}\alpha IQ^2\right\}\cos(\omega t) - G\left\{Q - \frac{3}{4}\alpha Q^3 - \frac{3}{4}\alpha I^2 Q\right\}\sin(\omega t) \\
&= I'\cos(\omega t) - Q'\sin(\omega t)
\end{aligned}
$$

This expression is used in Chapter 6 to determine the simulation model of the amplifier model.

Appendix D
Abbreviations

Table 4: Abbreviations

Abbreviation	Description
ADC	Analogue-to-digital conversion, analogue-to-digital converter
AGC	Automatic gain control
ASK	Amplitude shift keying
BER	Bit error rate
BPF	Band-pass filter
BPSK	Binary phase shift keying
CP	Compression point
CPE	Common phase error
CSMA/CA	Carrier sense multiple access with collision avoidance
DAC	Digital-to-analogue conversion, digital-to-analogue converter
DSSS	Direct sequence spread spectrum
FEC	Forward error correction
FFT	Fast Fourier transform
FHSS	Frequency hopping spread spectrum
FSK	Frequency shift keying
IC	Integrated circuit
ICI	Inter-channel interference
IF	Intermediate frequency
IFFT	Inverse fast Fourier transform
IP3	Third order intercept point
IR	Infrared
ISI	Inter-symbol interference
ISM	Industrial, scientific and medical
LAN	Local area network
LLC	Logical link control
LNA	Low noise amplifier
LPF	Low-pass filter
MAC	Medium access control
OFDM	Orthogonal frequency division multiplexing
OSI	Open systems interconnection
PA	Power amplifier
PAD	Power amplifier driver
PAP	Peak-to-average power
PHY	Physical layer
PLCP	Physical layer convergence procedure
PMD	Physical medium dependent
PSD	Power spectral density
PSK	Phase shift keying

Abbreviation	Description
QAM	Quadrature amplitude modulation
QPSK	Quadrature phase shift keying
RF	Radio frequency
SAW	Surface acoustic wave
SER	Symbol error rate
SNR	Signal-to-noise ratio
U-NII	Unlicensed national information infrastructure
VGA	Variable gain amplifier
WLAN	Wireless local area network

Appendix E
References

[1] Maddocks, M. C. D., "An Introduction to Digital Modulation and OFDM Techniques," Research Department Report RD1993/10, British Broadcasting Corporation, 1993.
http://www.bbc.co.uk/rd/pubs/reports/1993-10.pdf

[2] Rappaport, T. S., *Wireless Communications: Principles and Practice*, Upper Saddle River: Prentice-Hall, 1996.

[3] Van Nee, R. and Prasad, R., *OFDM for Wireless Multimedia Communications*, London: Artech House, 2000.

[4] Stott, J. H., "The Effects of Phase Noise in COFDM," Research Department, British Broadcasting Corporation, 1998.
http://www.bbc.co.uk/rd/pubs/papers/pdffiles/jsebu276.pdf

[5] Côme, B., et al., "Impact of Front-end Non-idealities on Bit Error Rate Performance of WLAN-OFDM Tranceivers," *Microwave Journal*, pp. 126-140, February 2001.

[6] Kaitz, T., "Performance Aspects of OFDM PHY Proposal," IEEE 802.16 Broadband Wireless Access Working Group, IEEE 802.16.3c-01/49, 2001.
http://www.ieee802.org/16/tg3/contrib/802163c-01_49.pdf

[7] Stott, J. H., "The Effects of Frequency Errors in OFDM", Research Department Report RD1995/15, British Broadcasting Corporation, 1995.
http://www.bbc.co.uk/rd/pubs/reports/1995-15.pdf

[8] Speth, M., et al., "Optimum Receiver Design for Wireless Broad-Band Systems Using OFDM—Part I," *IEEE Transactions on Communications*, Vol. 47, No. 11, pp. 1668-1677, November 1999.

[9] Schmidl, T. M. and Cox, D. C., "Robust Frequency and Timing Synchronization for OFDM," *IEEE Transactions on Communications*, Vol. 45, No. 12, pp. 1613-1621, December 1997.

[10] Bing, B., *High-speed Wireless ATM and LANs*, London: Artech House, 2000.

[11] O'Hara, B. and Petrick, A., *The IEEE 802.11 Handbook: A Designer's Companion*, New York: IEEE Press, 1999.

[12] *Supplement to IEEE Standard for Information Technology—Telecommunications and Information Exchange between Systems—Local and Metropolitan Area Networks—Specific Requirements—Part 11: Wireless LAN Medium Access Control (MAC) and Physical Layer (PHY) Specifications: High-speed Physical Layer in the 5 GHz Band*, New York: IEEE Press, 1999.

[13] Apeldoorn, R., "HomeRF-MM System Implications for Different DAC Solutions in the TAHOE," Internal Laboratory Report RVA/IR00001.0, Philips Semiconductors, 2000.

[14] "Prelimenary IF Chip Requirements for a 1.490 GHz High Performance IF OFDM Chip Intended for IEEE 802.11a 5.x GHz OFDM WLAN Systems," Philips Semiconductors, 2001.

[15] Huang, X., "On Transmitter Gain/Phase Imbalance Compensation At Receiver," *IEEE Communications on Letters*, Vol. 4, No. 11, pp. 363-365, November 2000.
[16] Gardner, F. M. and Baker, J. D., *Simulation Techniques: Models of Communication Signals and Processes*, Chichester: Wiley-Interscience, 1997.
[17] Van den Bos, C. et al., "Effects of Smooth Non-linear Distortion on OFDM BER," *Proceedings of the IEEE International Symposium on Circuits and Systems*, Vol. 4, pp. 469-472, 2000.
[18] Liu, C.-L., "The Effect of Nonlinearity on a QPSK-OFDM-QAM Signal," *IEEE Transactions on Consumer Electronics*, Vol. 43, No.3, pp. 443-447, August 1997.
[19] Velthuis, W. R., "Device Specification Document for Onyx2_V2," Lucent Technologies, 2000.
[20] "Preliminary XF5060PA-S02501 PA MMIC for 5.0 GHz – 6.0 GHz Wireless Communication," Murata, 2000.
[21] Shanmugam, K. S., *Digital and Analog Communication Systems*, Singapore: John Wiley & Sons, 1985.
[22] Anderson, R. W., et al., "S-Parameter Techniques for Faster, More Accurate Network Design," Test & Measurement Application Note 95-1, Hewlett-Packard, 1997.
http://www.tm.agilent.com/data/static/eng/tmo/Notes/interactive/an-95-1/